The Geological Society of America
Special Paper 524

High-resolution multiproxy cyclostratigraphic analysis of environmental and climatic events across the Cretaceous-Paleogene boundary in the classic pelagic succession of Gubbio (Italy)

Matthias Sinnesael*
Earth System Science, Analytical, Environmental and Geo-Chemistry (AMGC), Vrije Universiteit Brussel, Pleinlaan 2, B-1050 Brussels, Belgium

David De Vleeschouwer
Earth System Science, Analytical, Environmental and Geo-Chemistry (AMGC-WE), Vrije Universiteit Brussel, Pleinlaan 2, B-1050 Brussels, Belgium, and MARUM (Zentrum für Marine Umweltwissenschaften der Universität Bremen), Universität Bremen, Leobener Strasse, D-28359, Bremen, Germany

Rodolfo Coccioni
Dipartimento di Scienze Pure e Applicate, Università degli Studi di Urbino "Carlo Bo," Campus Scientifico, Località Crocicchia, 61029 Urbino, Italy

Philippe Claeys
Earth System Science, Analytical, Environmental and Geo-Chemistry (AMGC-WE), Vrije Universiteit Brussel, Pleinlaan 2, B-1050 Brussels, Belgium

Fabrizio Frontalini
Dipartimento di Scienze Pure e Applicate, Università degli Studi di Urbino "Carlo Bo," Campus Scientifico, Località Crocicchia, 61029 Urbino, Italy

Luigi Jovane
Instituto Oceanografico, Universidade de São Paulo, 05508–090 São Paulo, Brazil

Jairo F. Savian
Departamento de Geologia, Instituto de Geociências, Universidade Federal do Rio Grande do Sul, Avenida Bento Gonçalves 9500, 91501-970 Porto Alegre, Brazil

Alessandro Montanari
Osservatorio Geologico di Coldigioco, Contrada Coldigioco 4, 62021 Apiro, Italy

*Corresponding author: masinnes@vub.ac.be.

Sinnesael, M., De Vleeschouwer, D., Coccioni, R., Claeys, P., Frontalini, F., Jovane, L., Savian, J.F., and Montanari, A., 2016, High-resolution multiproxy cyclostratigraphic analysis of environmental and climatic events across the Cretaceous-Paleogene boundary in the classic pelagic succession of Gubbio (Italy), *in* Menichetti, M., Coccioni, R., and Montanari, A., eds., The Stratigraphic Record of Gubbio: Integrated Stratigraphy of the Late Cretaceous–Paleogene Umbria-Marche Pelagic Basin: Geological Society of America Special Paper 524, doi:10.1130/2016.2524(09).

ABSTRACT

We studied a high-resolution multiproxy data set, including magnetic susceptibility (MS), $CaCO_3$ content, and stable isotopes ($\delta^{18}O$ and $\delta^{13}C$), from the stratigraphic interval covering the uppermost Maastrichtian and the lower Danian, represented by the pelagic limestones of the Scaglia Rossa Formation continuously exposed in the classic sections of the Bottaccione Gorge and the Contessa Highway near Gubbio, Italy. Variations in all the proxy series are periodic and reflect astronomically forced climate changes (i.e., Milankovitch cycles). In particular, the MS proxy reflects variations in the terrigenous dust input in this pelagic, deep-marine environment. We speculate that the dust is mainly eolian in origin and that the availability and transport of dust are influenced by variations in the vegetation cover on the Maastrichtian-Paleocene African or Asian zone, which were respectively located at tropical to subtropical latitudes to the south or far to the east of the western Tethyan Umbria-Marche Basin, and were characterized by monsoonal circulation. The dynamics of monsoonal circulation are known to be strongly dependent on precession-driven and obliquity-driven changes in insolation. We propose that a threshold mechanism in the vegetation coverage may explain eccentricity-related periodicities in the terrigenous eolian dust input. Other mechanisms, both oceanic and terrestrial, that depend on the precession amplitude modulated by eccentricity, can be evoked together with the variation of dust influx in the western Tethys to explain the detected eccentricity periodicity in the $\delta^{13}C$ record. Our interpretations of the $\delta^{18}O$ and MS records suggest a warming event ~400 k.y. prior to the Cretaceous-Paleogene (K-Pg) boundary, and a period of climatic and environmental instability in the earliest Danian. Based on these multiproxy phase relationships, we propose an astronomical tuning for these sections; this leads us to an estimate of the timing and duration of several late Maastrichtian and Danian biostratigraphic and magnetostratigraphic events.

INTRODUCTION

The Cretaceous-Paleogene (K-Pg) boundary was first defined biostratigraphically by Luterbacher and Premoli Silva (1964) on the basis of planktonic foraminifera in the Bottaccione section near Gubbio, Italy. The K-Pg boundary represents one of the most debated biotic crises in Earth's history, most notably the complete extinction of the dinosaurs, non-turtle marine reptiles, ammonites, and the shallow-water rudists, as well as almost all calcareous nannoplankton and planktonic foraminifera, among which only four dwarf foraminiferal species survived the mass extinction (e.g., Smit, 1982; Olsson et al., 1996; Huber et al., 2002; Arenillas et al., 2006; Schulte et al., 2010, and references therein). The discovery of an iridium anomaly precisely at the K-Pg boundary in the Spanish section of Caravaca by Smit and Hertogen (1980), and in several sections in the Umbria-Marche Basin of Italy (including Gubbio) by Alvarez et al. (1980), opened the way to the hypothesis that the mass extinction was caused by the catastrophic impact of a large extraterrestrial object, a comet or an asteroid, on the Earth's surface. The discovery of the giant Chicxulub impact structure in the Yucatán Peninsula by Hildebrand et al. (1991) and the radioisotopic dating of impact melt rocks and related impact glasses found in K-Pg boundary sections in the Caribbean and Gulf of Mexico regions by Swisher et al. (1992), made the impact hypothesis widely accepted and ended an era of speculations about what could have triggered the K-Pg boundary biotic crisis (e.g., Schulte et al., 2010, and references therein).

The time period immediately preceding the K-Pg event is characterized by a temporary perturbation of global environmental conditions, possibly related to the second (main) phase of the Deccan basaltic volcanism (e.g., Courtillot and Renne, 2003; Chenet et al., 2007; Schoene et al., 2015), which terminated a long period of relatively stable and generally warm climate. Osmium (Os) isotope analysis in deep-sea sedimentary successions suggests that the main second stage of Deccan volcanism preceded the K-Pg boundary by a few hundred thousand years (Ravizza and Peucker-Ehrenbrink, 2003; Ravizza, 2007). From these studies stems the hypothesis that the Deccan flood basalt volcanism produced large volumes of gases, which likely caused severe perturbations of the atmosphere with consequential change of the global climate (Nordt et al., 2003; Wilf et al., 2003; Self et al., 2008; Keller et al., 2012).

The aftermath of the K-Pg event is characterized by a recovery period (e.g., D'Hondt et al., 1998; Coxall et al., 2006) and the occurrence of multiple hyperthermal events; the Paleocene-Eocene Thermal Maximum is the most prominent example (e.g., Lourens et al., 2005). Investigating the temporal dimension of these climatic events, and possibly their relationship with insolation forcing (e.g., Lourens et al., 2005), enables a better

understanding of the Paleogene climate system, and the changes eventually induced by the K-Pg boundary event and their extent.

In this paper we utilize high-resolution multiproxy data including bulk-rock $CaCO_3$ (a proxy for calcareous plankton productivity), magnetic susceptibility (MS; a proxy for terrigenous influx), together with carbon and oxygen stable isotopes, as the basis for a cyclostratigraphic analysis of the K-Pg transition in the classic sections of the Bottaccione Gorge and the Contessa Valley near Gubbio. This allows a better understanding of the climatic changes that were occurring through this critical geological time interval, not only as a consequence of background orbital forcing, but also of such exceptional events as the Deccan volcanism and the K-Pg boundary impact. In addition, we used the outputs of our multiproxy cyclostratigraphic analysis to improve the relative chronology of these environmental-climatic events and propose a numerical astrochronologic time scale for the magnetobiostratigraphy of the upper Maastrichtian to upper Danian interval.

GEOLOGICAL AND STRATIGRAPHIC BACKGROUND

The studied stratigraphic sections are located in the Umbria region of the northeastern Apennines, near the medieval town of Gubbio, Italy (Fig. 1A). The Umbria-Marche pelagic paleobasin (Fig. 1B) was part of a microplate of African continental crust, the so-called Adriatic Promontory or Adria (Channell et al., 1979), and was the last part of Adria to be involved in the Alpine orogenic phase that brought the deformation of the Apennines fold and thrust belt. The Umbria-Marche Basin has an exceptionally continuous ~2-km-thick sedimentary succession of pelagic carbonates that spans the early Jurassic to the middle Miocene. The Scaglia Rossa Formation represents the middle part of such a pelagic succession, from the earliest Turonian to the latest Ypresian (e.g., Montanari et al., 1989, and references therein). It is a characteristically pink biomicritic limestone made up of planktonic foraminiferal tests suspended in a coccolith matrix with a terrigenous component of silt and clay considered to be of eolian origin (Arthur and Fischer, 1977; Johnsson and Reynolds, 1986). The concentration of the terrigenous fraction varies from as little as 2 wt% to 60 wt% in marly intervals. The lower R1 member of the Scaglia Rossa (Turonian to Santonian) and the upper Ypresian R4 member of this formation contain intercalations of radiolarian nodular chert layers (Montanari et al., 1989). The Campanian to Maastrichtian R2 member of the Scaglia Rossa is devoid of chert and marly sediments, except for a short marly interval at its base (the R2m member in Montanari et al., 1989). The Danian to Thanetian R3 member is characterized by a number of marly horizons interbedded with the typical pelagic limestones of this formation. The Scaglia Rossa also records regional synsedimentary extensional tectonic activity, which started in the early Turonian, peaked in the Danian, and diminished and ended in the Ypresian. Such a tectonic phase led to the formation of gentle intrabasinal depocenters bound by synsedimentary normal faults, into which seismoturbidites made up of reworked pelagic ooze were deposited, along with soft sediment slump masses (Alvarez and Lowrie, 1984; Alvarez et al., 1985; Montanari et al., 1989; Bice et al., 2007). With the exception of slump structures in the early Campanian (foraminiferal *Contusotruncana plummarae* Zone) and possibly in the early Danian (foraminiferal P1b Zone), in the Bottaccione section, neither turbidites nor sedimentary disturbances occur throughout the Scaglia Rossa succession. This study focuses on the uppermost Cretaceous R2 and the lowermost Paleocene R3 members of the Scaglia Rossa Formation, which are exposed in the Bottaccione Gorge and in the Contessa Valley of Gubbio, respectively (Fig. 1A). We use this composite because of probable slump structures in the early Danian Bottaccione section and a retaining stone wall that covers the uppermost Maastrichtian Contessa section.

A complete record of data from the stratigraphic interval we studied is shown in Figure 2. Figures 2A and 2B show the actual outcrops of the K-Pg transition in the Contessa Highway and Bottaccione Gorge sections, respectively. Figure 2C is a composite integrated biomagnetostratigraphic scheme for this interval, as derived from published studies, and described in detail by Coccioni et al. (2016, and references therein). Figure 2D shows the plots of the actual multiproxy series we used in this study, highlighting the main environmental and climatic events recorded through this stratigraphic interval.

MATERIALS AND METHODS

We sampled the Bottaccione Gorge section, i.e., the upper 7.2 m of the Maastrichtian, at regular 5 cm intervals using an electric drill with a masonry tungsten drill bit. We produced ~40 g of fine rock powder per sample, ultimately dry sieved with a 250 μm sieve for later calcimetric and stable isotope analyses. Calcium carbonate content (weight percent $CaCO_3$) was measured at the Osservatorio Geologico di Coldigioco (Italy) with a Dietrich-Frühling water calcimeter with a precision of ±2.5%. Calibration was done every 20 samples using a Carrara marble standard. The MS ($m^3\ kg^{-1}$) in bulk powdered rock was measured at the Osservatorio Geologico di Coldigioco with a Bartington MS-2B Dual Frequency magnetometer, averaging 3 measurements for each sample and applying mass correction. Stable isotope measurements of the bulk carbonate rock for $\delta^{13}C$ (‰ Vienna Peedee belemnite, VPDB) and $\delta^{18}O$ (‰ VPDB) were carried out at the Vrije Universiteit Brussel (Belgium) using both a dual inlet Thermo Finnigan Delta^{plus}XL isotope ratio mass spectrometer (IRMS), interfaced with an automated Kiel III device for carbonates, and a Nu Perspective IRMS interfaced with a Nu Carb automated carbonate device. Acidification of the samples occurred at a temperature of 70 °C for both instruments. Calibration was carried out using NCM standards (+2.09‰ VPDB, -1.90‰ VPDB). On the basis of replicated measurements on sampled material, the reproducibility for both mass spectrometers on the carbon and oxygen isotopes was estimated as 0.05‰ (1σ) and 0.15‰ (1σ), respectively.

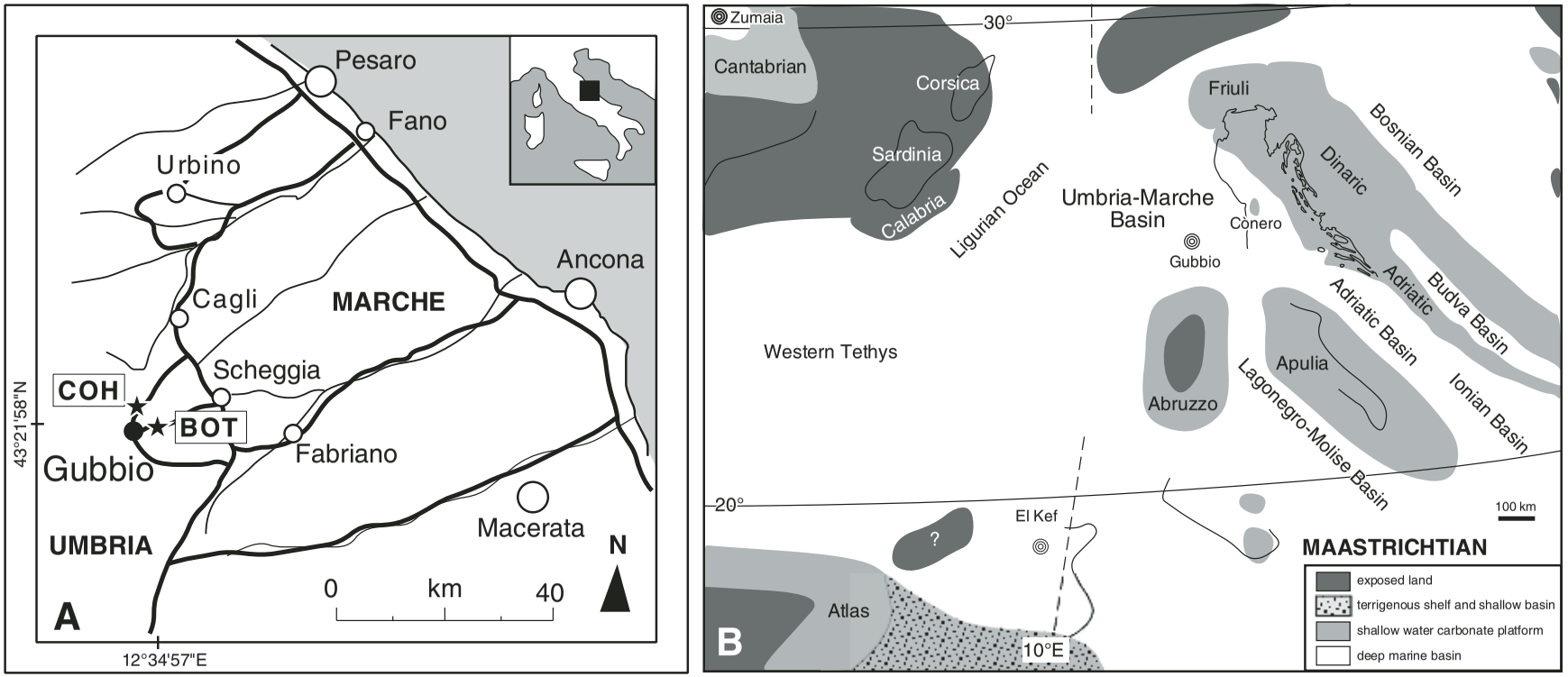

Figure 1. (A) Geographical location of the stratigraphic sections near the town of Gubbio, Italy. COH—Contessa Highway section; BOT—Bottaccione section. (B) Maastrichtian paleogeography of the western Mediterranean region with the location of the Gubbio sections in the Umbria-Marche pelagic basin, simplified and redrawn from Dercourt et al. (1993), Rosenbaum et al. (2002), and Adatte et al. (2002).

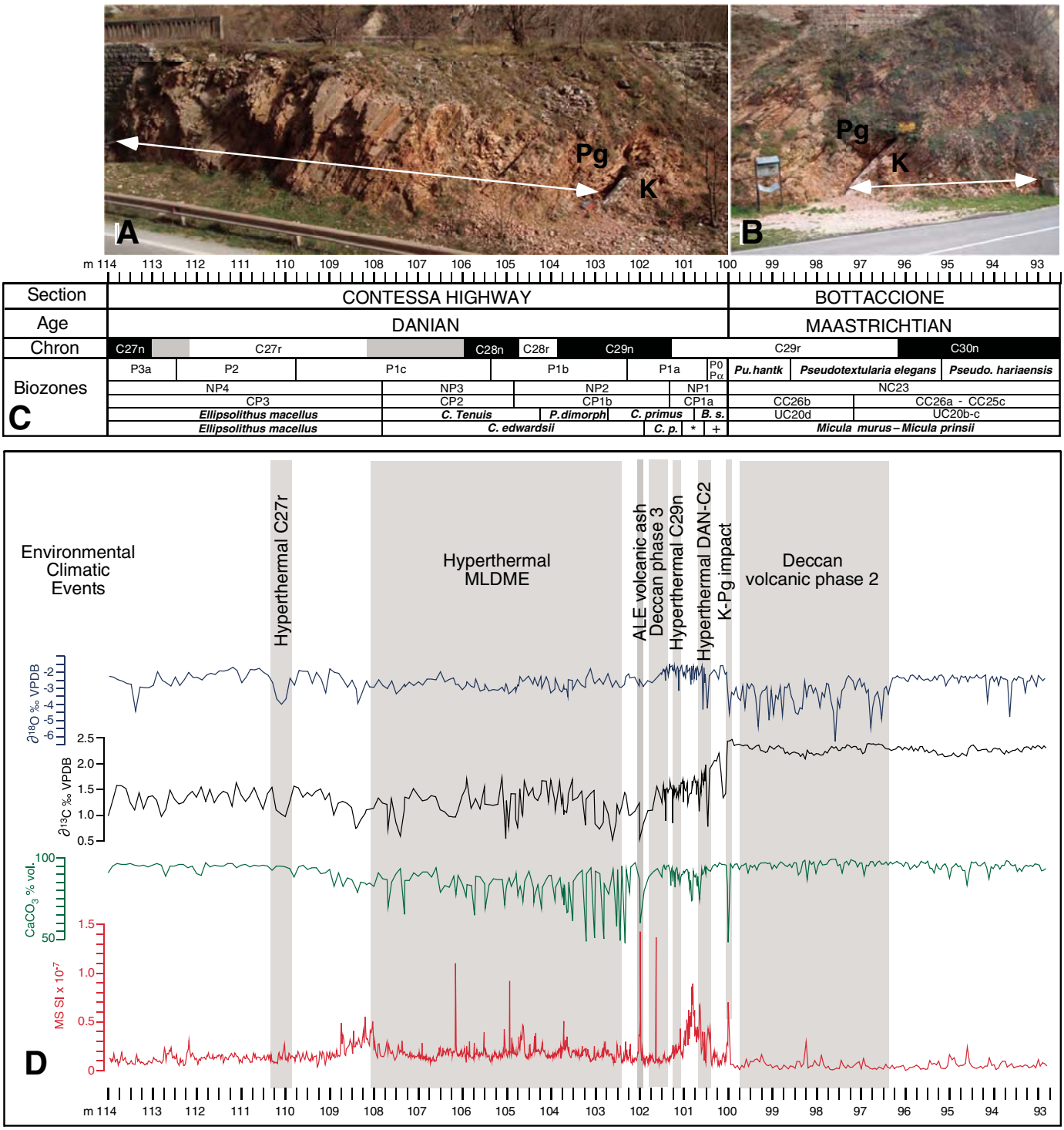

Figure 2. (A) The Contessa Highway section (COH; indicated by the white arrow). (B) Bottaccione section (BOT; white arrow), as indicated by the white double arrow lines (C). Biomagnetostratigraphy of BOT, COH sections. Magnetostratigraphy is according to Roggenthen and Napoleone (1977); the BOT magnetostratigraphy is according to Lowrie et al. (1982). The detailed biostratigraphy for the COH section is from Coccioni et al. (2012b), whereas that for the BOT section is from Coccioni and Premoli Silva (2015). * indicates 1.05–0.95 *F. petalosa*; 0.95 m–0.75 m *C. ultimus*; 0.75 m—0.55 m *B.? parvulum*; + indicates 0.55 m–0 m Barren Interval; + *B.? romeinii.* (D) Multiproxy series used for the cyclostratigraphic analysis of the composite BOT-COH section. The oxygen stable isotopes $\delta^{18}O$ (‰), carbon stable isotopes $\delta^{13}C$ (‰), and $CaCO_3$ (wt%) content for the COH section are from Coccioni et al. (2012a), while the high-resolution MS intensity series is from this work, along with all the proxy series for the BOT section. K-Pg—Cretaceous-Paleogene; VPDB—Vienna Peedee belemnite; MLDME—Middle–Lower Danian multiple event.

A collection of 1 cm spaced bulk-rock samples from the lower half of the Contessa Highway section (the lower 7 m of the Danian), and 2 cm spaced samples for the upper half of the section, a total of 1049 samples, were measured for MS with a Kappabridge KLY-2 MS meter at the National Oceanographic Centre Southampton (University of Southampton, UK). As for the $CaCO_3$ and stable isotope proxies for the Contessa Highway section, we utilized the data published by Coccioni et al. (2012a). In this dataset, sample spacing ranges between 2 and 10 cm. We conducted spectral analyses of the various proxy series (MS, $CaCO_3$ content, $\delta^{18}O$, and $\delta^{13}C$) separately for the Bottaccione Gorge and Contessa Highway sections in Matlab using fast Fourier transform (FFT) periodogram algorithms modified from Muller and MacDonald (2000). This periodogram method was successfully used for cyclostratigraphic analysis of portions of the Umbria-Marche stratigraphic succession by Cleaveland et al. (2002), Mader et al. (2004), Brown et al. (2009), and Hyland et al. (2009), and explained in detail by Bice et al. (2012). We performed FFTs of the data (detrended and padded with zeros) in the stratigraphic domain, which yielded a set of spectral peaks representing the stratigraphic wavelengths (periods) of the cycles. We evaluated the statistical significance of spectral peaks by generating a 95% confidence level (c.l.) from a Monte Carlo noise simulation (Muller and MacDonald, 2000). The persistence of the spectral peaks through the stratigraphic section was evaluated through the use of an evolutionary, or sliding window, FFT. The window size was chosen to be about one-third of the entire stratigraphic interval analyzed, large enough to enable the detection of short and long eccentricity signals given the sedimentation rates estimated for the studied intervals.

Astronomical tuning and ultimate astrochronologic dating of the magnetostratigraphic, biostratigraphic, environmental, and climatic events recorded in the composite Bottaccione–Contessa Highway section (BOT-COH; Fig. 2C) was accomplished through the use of broad bandpass filtering of the high-resolution MS proxy series. Variations in MS proxy series between ~300 and 500 k.y. were isolated for the long eccentricity (405 k.y.) band. These filtered data were then used for correlation via constrained pattern matching with the theoretical eccentricity curve of La2011 (Laskar et al., 2011). We performed the actual tuning of the composite section by correlating the maxima of a broad ~300–500 k.y. bandpass curve of the MS time series with the maxima of the bandpass eccentricity curve of La2011.

CYCLOSTRATIGRAPHIC ANALYSIS

Bedding Style: Homogenites versus Rhythmites

In the Umbria-Marche pelagic basin, rhythmite sequences (i.e., a rhythmic alternation of limestone and marl layers) are mainly found in the late Paleocene to Neogene part of the sedimentary succession (e.g., the Oligocene Scaglia Cinerea Formation of Hyland et al., 2009; or the Serravallian Schlier Formation of Cleaveland et al., 2002). The sequences reflect the time when, due to the peri-Adriatic orogenic phase, the Umbria-Marche pelagic basin, which was then at a middle latitude of ~40°N and in a genuine glacio-eustatic climatic system, began receiving a significant amount of fine-grained terrigenous material, mainly derived from the erosion and runoff from the emerging Alps and the northwestern Apennines orogenic belts. Rhythmite series are also found in the Cenomanian Scaglia Bianca Formation, where the rhythmicity is given by cyclic alternations of foraminiferal-coccolith limestones and radiolarian cherts, readily recognizable in the field (e.g., Beaudoin et al., 1996; Mitchell et al., 2008; Batenburg et al., 2016). However, the Scaglia Rossa Formation does not exhibit a visibly outstanding rhythmite character. The limestones of this formation are mostly made up of biomicritic ooze homogenized by synsedimentary bioturbation (Arthur and Fischer, 1977). Nevertheless, Scaglia Rossa outcrops show well-bedded limestones, with an apparent bed thickness between 5 and 20 cm; however, what appears at first sight to be bedding is in reality pseudobedding, i.e., the partitioning of the homogenized pelagic biomicrite by often anastomizing plane-parallel stylolites, which are denoted by millimeter-thick residual clay seams (Alvarez et al., 1985). These stylolites formed in the homogeneous calcareous sediment in a process of calcium carbonate pressure solution during late diagenesis in response to burial and sediment loading, thus with a principal stress component normal to the paleohorizontal plane (Alvarez et al., 1985, and references therein). This pressure solution process occurs preferably, but not always, along horizons of a slightly contrasting composition within the otherwise apparently homogeneous sediment. Consequently, the pseudobedding of the Scaglia Rossa does not reflect variations in sedimentation possibly related to climatic changes, and therefore it is not suited for cyclostratigraphic and astrochronologic analyses. For this reason we sampled the Gubbio sections at closely spaced intervals to produce proxy series reflecting variations in sedimentary and paleoenvironmental characteristics. These proxies are total content of calcium carbonate, which is mostly biogenic $CaCO_3$ derived from planktonic foraminifera and calcareous nannofossils, MS imparted by the terrigenous component of the sediment, and oxygen ($\delta^{18}O$) and carbon ($\delta^{13}C$) isotopes, which reflect variations in the composition of seawater.

Bottaccione Section

The cyclic character of the terminal Maastrichtian limestone succession at Gubbio is well manifested in the spectral analysis (FFT) outputs shown in Figure 3, whereas the details of cyclic variations of the proxies and their phase relation are shown in

Figure 3. Fast Fourier transform (FFT) outputs of the multiproxy cyclostratigraphic analysis for the terminal Maastrichtian interval of the Bottaccione (BOT) section. (A) Magnetic susceptibility (MS); c.l.—confidence level; ETP—eccentricity, tilt, precession; sed.—sedimentation. (B) $CaCO_3$ (wt%). (C) Oxygen stable isotopes ($\delta^{18}O‰$). (D) Carbon stable isotopes ($\delta^{13}C‰$).

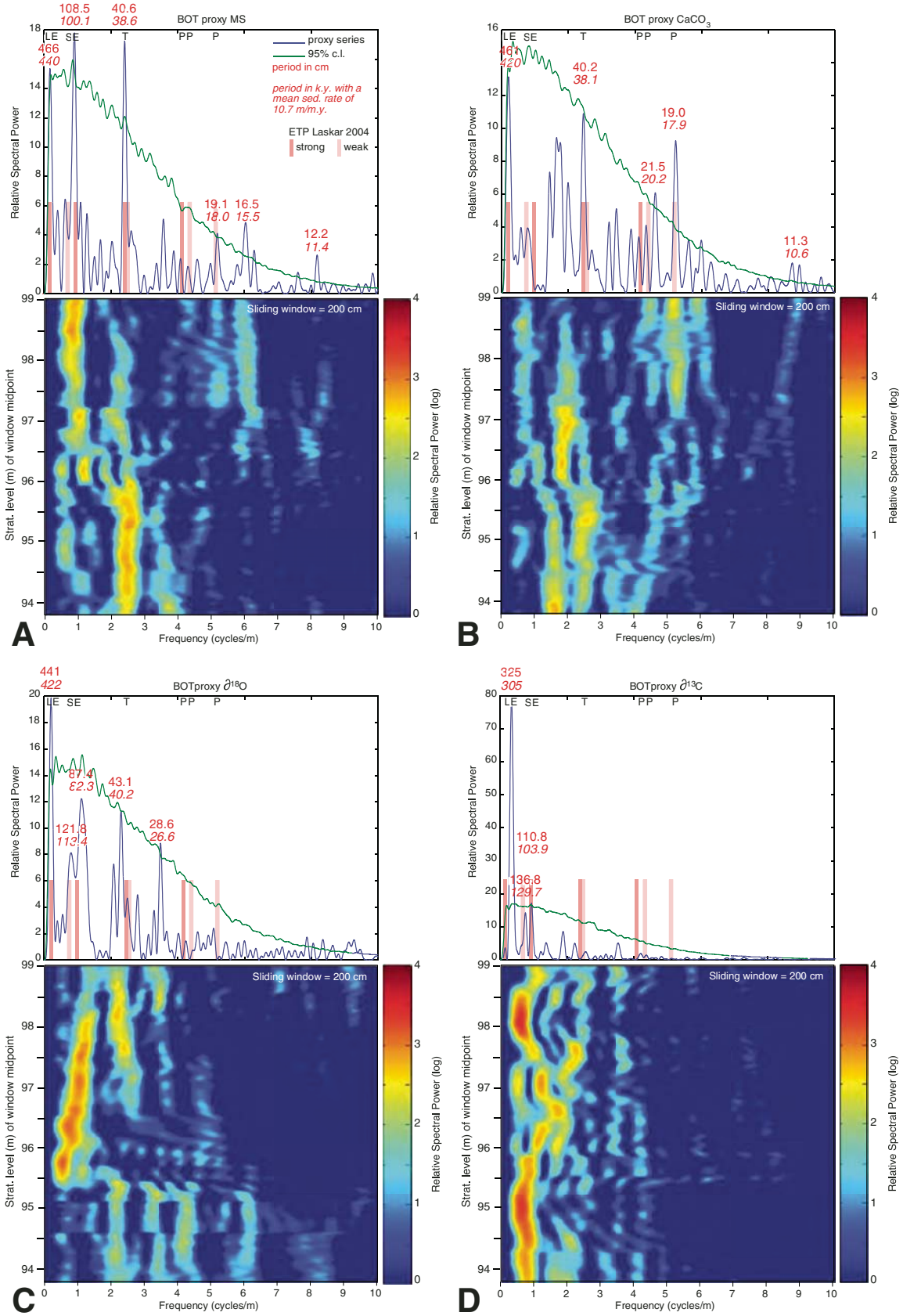
BOT proxy MS
BOT proxy CaCO3
BOTproxy ∂18O
BOTproxy ∂13C
LE SE T PP P
proxy series
95% c.l.
period in cm
period in k.y. with a mean sed. rate of 10.7 m/m.y.
ETP Laskar 2004
strong
weak
Relative Spectral Power
Sliding window = 200 cm
Strat. level (m) of window midpoint
Relative Spectral Power (log)
Frequency (cycles/m)
A
B
C
D

Figure 3.

Figure 4. The mean sedimentation rate estimated by various approaches for the uppermost Maastrichtian in the Bottaccione section (e.g., Arthur and Fischer, 1977; Lowrie et al., 1990; Mukhopadhyay et al., 2001; Gardin et al., 2012; Wendler, 2013; Husson et al., 2014), is ~10 m m.y.$^{-1}$. This mean value is generally confirmed by our cyclostratigraphic analysis despite the fact that the FFT power spectra of the four proxy series do not manifest equally strong frequency signatures. The MS series, for example (Fig. 3A), yielded an overall red noise spectrum with significant frequency peaks (i.e., reaching or surpassing a 95% c.l.) having periods consistent with Milankovitch eccentricity (long and short), tilt (obliquity), and precession (ETP) cycles, as determined in the astronomical solution of Laskar et al. (2004). In particular, the powerful frequency peak with a period of 40.6 cm (Fig. 3A) would yield a period of 38.6 k.y. assuming a mean sedimentation rate of 10.7 m m.y.$^{-1}$, which is the period of the tilt in the ETP solution of Laskar et al. (2004) for the time interval encompassing the K-Pg boundary between 68 and 62 Ma. Weak but still statistically significant peaks appear at higher frequencies (with periods of ~16, 13, and 12 cm), which, nevertheless, seem to be recorded only in the upper half of the Bottaccione Gorge section (see sliding window FFT plot in Fig. 3A). It can be speculated that these high-frequency signals derive from local compositional disturbances, possibly caused by pressure-solution stylolites, which have a frequency much higher than the period of ~20 cm probably imparted by the precession cycle, as shown by a 17–27 cm bandpass filtered curve superimposed on the actual outcrop face in Figure 4A. The weight percent $CaCO_3$ proxy has an antiphase relation in respect to the MS proxy (i.e., a relatively high weight percent $CaCO_3$ value corresponds to a relatively low MS value), as expected, and it is clearly shown in the sample to sample plot in Figure 4B, and in the bandpass filter correlations in Figures 4C and 4D. Nevertheless, the FFT power spectra of weight percent $CaCO_3$, as shown in Figure 3B, look somewhat different from the MS spectra. The precession frequency signals are better defined than in the MS spectrum, while the tilt signal is practically identical to the one of the MS series. On the other hand, the short eccentricity signal is weak. The stable isotope series ($\delta^{18}O$ and $\delta^{13}C$) both yielded very noisy spectra in which only the low-frequency signals, possibly long and short eccentricity, appear distinctively elevated, but still do not reach the 95% c.l. in the $\delta^{18}O$ (Fig. 4C), and barely reach it in the $\delta^{13}C$ series (Fig. 4D). The frequency signal of the tilt is well represented in both the MS and weight percent $CaCO_3$ series and is centered at about a 40 cm period. It also appears at the top and bottom of the section in the $\delta^{18}O$ signal, but is practically absent in the carbon stable isotope series (Fig. 4). The results for the carbon stable isotope series are similar to those of Voigt et al. (2012).

Contessa Highway section

The Contessa Highway section (Coccioni et al., 2012a, 2012b) covers in continuity the lower 14 m of the total 15 m thickness of the Danian of the composite Paleogene Gubbio succession (Coccioni et al., 2012b). The mean sedimentation rate for this Scaglia Rossa R3 member interval was estimated as ~4 m m.y.$^{-1}$ by Coccioni et al. (2012b) based on the ages of magnetic polarity reversals, which were defined for this section by Lowrie et al. (1982), and given by the geologic time scale of Gradstein et al. (2004). This value is lower than the ~10 m m.y.$^{-1}$ estimated for the underlying Maastrichtian R2 member. The drop in sedimentation rate is also observed at other K-Pg boundary sections and can be explained as a function of the reduction of calcium carbonate by marine plankton and the decrease of organic carbon fluxes toward the deep sea (Herbert and D'Hondt, 1990; D'Hondt et al., 1998; D'Hondt, 2005). For this section, Coccioni et al. (2012a) provided data series for magnetic characteristics (MS, anisotropy of anhysteretic susceptibility, isothermal remanent magnetization, hard isothermal remanent magnetization), $CaCO_3$ (wt%), and stable isotopes as $\delta^{13}C$ (‰) and $\delta^{18}O$ (‰), with varying sample spacing through the section. For the lower 8.4 m of the section, the mean sample spacing was 5 cm, whereas for the rest of the section, the mean sample spacing was 10 cm. With a sample spacing of 5 cm, and a mean estimated sedimentation rate of ~4 m m.y.$^{-1}$, the short eccentricity can be reliably detected, but not the higher frequencies. A 10 cm sampling spacing, with the same estimated sedimentation rate, is too sparse for any significant cyclostratigraphic analysis. Aware of the limitations of these multiproxy series for a reliable spectral analysis, we resampled the entire Contessa Highway section at 1 cm sample spacing through the lower 7 m of the section, and at 2 cm spacing for the upper 7 m of the section. The 1049 collected samples were analyzed for MS; this new MS proxy series should be sufficiently dense to capture not only the relatively low frequencies of the short eccentricity and the tilt, but possibly also the precession cycle.

The cyclic character of the Danian limestone succession in the Contessa Highway section is synthesized in the spectral analysis (FFT) outputs shown in Figure 5, whereas the details of cyclic variations of the proxies and their phase relation are shown in Figure 6. The FTT power spectra of the new MS series (1–2 cm sample spacing) reveal a strong peak with a period of 176 cm, a series of 3 distinct peaks with periods spread between 37.5 and 48.6 cm barely reaching the 95% c.l., a sharp peak well elevated above the 95% c.l. with a period of 16.8 cm, and no significant signals in the high-frequency range (i.e., frequencies higher than 6 cycles/m) (Fig. 5A). Given a mean sedimentation rate of 4.3 m m.y.$^{-1}$, the suggestive peak with a period of 16.8 cm would represent a frequency period of 38.9 k.y., thus indistinguishable from the frequency of the tilt with a period 38.8 k.y. calculated by Laskar et al. (2004) for this astrochronologic time interval. Although relatively weak, this signal seems to be fairly stationary through the section (see sliding window FFT output in Fig. 5A), but weaker in the upper part of it, at around meter level 111–113 (where meter level 100 corresponds to the K-Pg boundary). Along the same line, and considering the same mean sedimentation rate of 4.3 m m.y.$^{-1}$, the 3 weak peaks in the frequency range of 43 ± 5 cm would correspond to a period around 100 k.y., which is

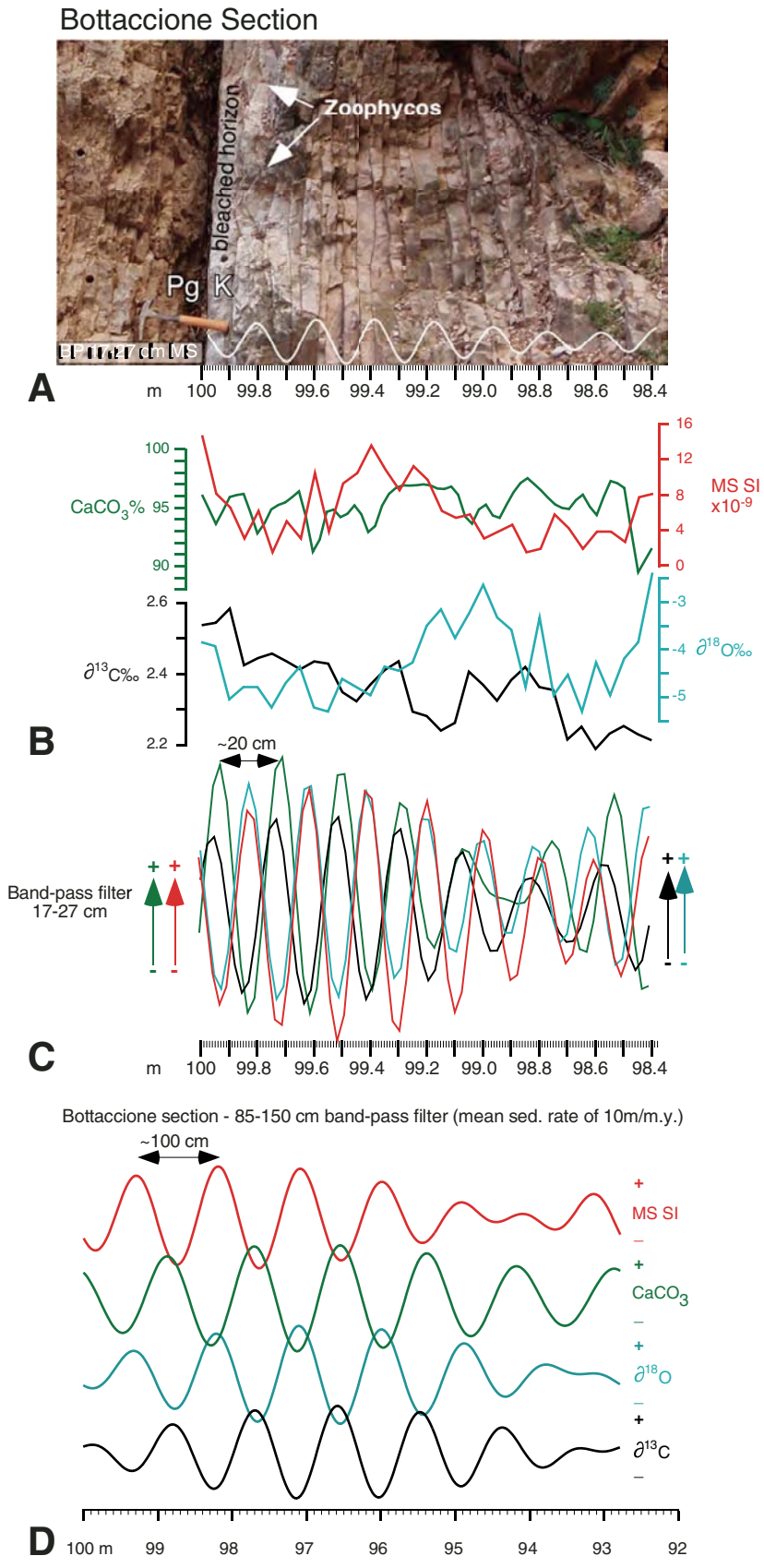

Figure 4. (A) Close-up outcrop view of the top 160 cm of the Maastrichtian R2 member of the Scaglia Rossa Formation in the Bottaccione section, with a superimposed bandpass (BP) curve (white sine line) for the magnetic susceptibility (MS) proxy with a filter of 17–27 cm, which represents the precession cycle. Pg—Paleogene; K—Cretaceous. (B) Plots of the actual multiproxy data series through the same stratigraphic interval. (C) BP curves for the 4 proxy series with a filter of 17–27 cm (precession cycle; sed.—sedimentation). (D) BP curves for the four proxy series with a filter of 85–150 cm that represent the short eccentricity cycle, through the entire 7.2 m terminal Maastrichtian stratigraphic interval studied in this work.

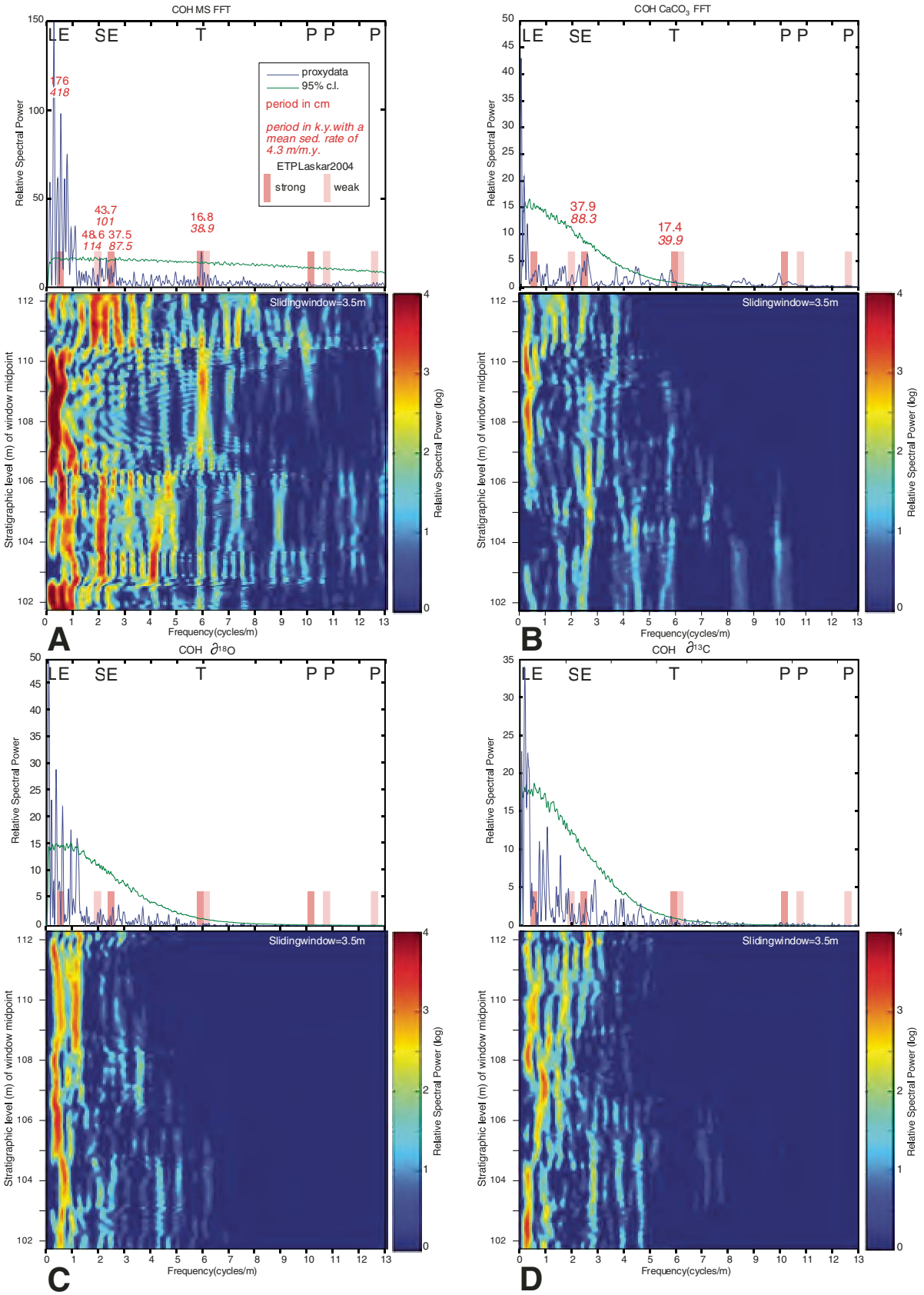
COH MS FFT
COH CaCO3 FFT
COH ∂18O
COH ∂13C
LE
SE
T
P P
P
proxydata
95% c.l.
period in cm
period in k.y.with a mean sed. rate of 4.3 m/m.y.
ETPLaskar2004
strong
weak
176
418
43.7
101
48.6
114
37.5
87.5
16.8
38.9
37.9
88.3
17.4
39.9
Slidingwindow=3.5m
Relative Spectral Power
Stratigraphic level (m) of window midpoint
Frequency(cycles/m)
Relative Spectral Power (log)
A
B
C
D

Figure 5.

Figure 5. Fast Fourier transform (FFT) outputs of the multiproxy cyclostratigraphic analysis for the Danian interval of the Contessa Highway section (COH). (A) Magnetic susceptibility (MS); c.l.—confidence level; ETP—eccentricity, tilt, precession; sed.—sedimentation. (B) $CaCO_3$ (wt%). (C) Oxygen stable isotopes ($\delta^{18}O$, ‰). (D) Carbon stable isotopes ($\delta^{13}C$, ‰). LE—Long Eccentricity; SE—Short Eccentricity; T—Tilt; P—Precession.

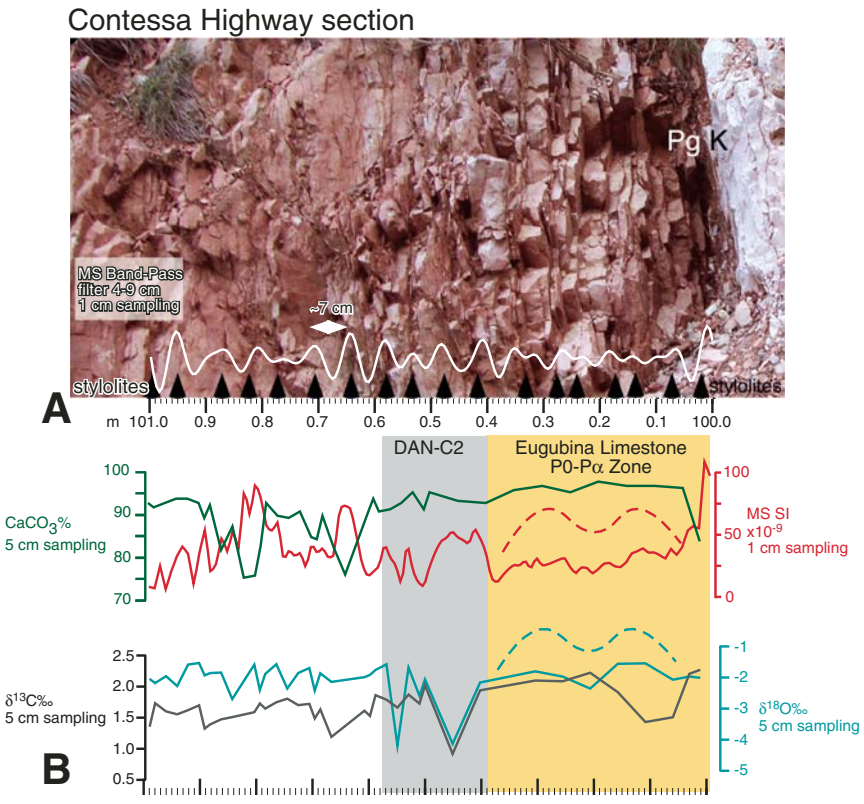

Figure 6. (A) Close-up outcrop view of the basal 10 cm of the Danian R3 member of the Scaglia Rossa Formation in the Contessa Highway section. Superimposed bandpass (BP) curve (white sine line) for the high-resolution magnetic susceptibility (MS) proxy series (1 cm sample spacing), with a filter of 4–9 cm, represents the precession cycle. Pg—Paleogene; K—Cretaceous. (B) Plots of the actual multiproxy data series through the same stratigraphic interval, with highlighted the intervals representing the Eugubina limestone (P0-Pα Zones), and the low $\delta^{18}O$ horizon reflecting the Dan-C2 hyperthermal event as in Coccioni et al. (2010). (C) BP curves for the 4 proxy series with a filter of 4–9 cm through the same 100 cm stratigraphic interval. (D) BP curves for the 4 proxy series with a filter of 36–63 cm, which represent the short eccentricity cycle, through the entire 14 m Danian stratigraphic interval studied in this work.

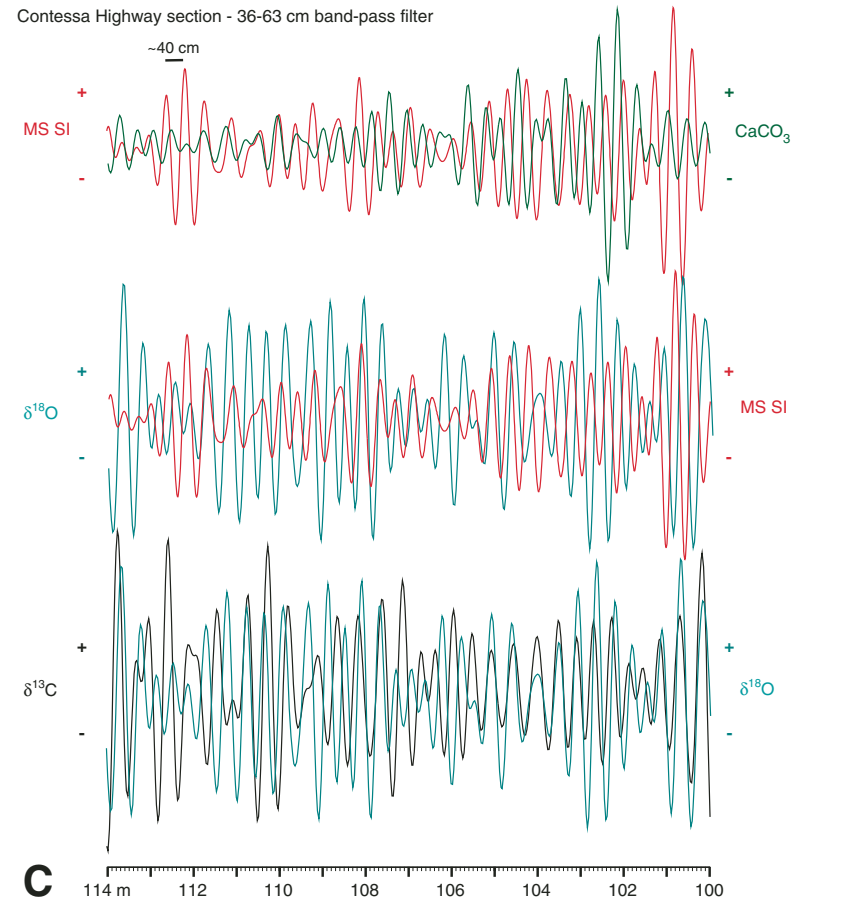

compatible with the dominant periods of the short eccentricity in both the solutions of Laskar et al. (2004, main periods of 94.2 k.y. and 98.7 k.y.), and Laskar et al. (2011, main periods of 95.1 k.y. and 99.9 k.y.). The FFT sliding window output in Figure 5A shows that through the lower part of the section, up to meter level 106, the central of these 3 peaks, with a period of 43.7 cm (equivalent to a period of 101 k.y. given a mean sedimentation rate of 4.3 m m.y.$^{-1}$), is the sole peak appearing with a moderate power and fair stationarity, whereas all 3 peaks are present only in the upper part of the section, above meter level 111. However, these short eccentricity signals are almost undetectable in the middle part of the section, between meter levels 106 and 111. The very strong peak with a period of 176 cm (equivalent to a period of 418 k.y. with a mean sedimentation rate of 4.3 m m.y.$^{-1}$), may represent the long eccentricity, which in the astronomical solutions of Laskar et al. (2004, 2011) has a mean period of 406 k.y. throughout the Danian.

As for the other three sparsely sampled proxy series ($CaCO_3$, $\delta^{13}C$, and $\delta^{18}O$), the FFT power spectra shown in Figures 5B–5D do not exhibit any significant signal in the high-frequency band. This is not surprising, because with a mean sedimentation rate of 4.3 m m.y.$^{-1}$, sampling at 5–10 cm mean intervals would not provide enough resolution to define precession cycles with expected periods in the range of 8.5 ± 1 cm. Nevertheless, in the $CaCO_3$ series (Fig. 5B) there is a weak signal elevated above the 95% c.l., with a period of 17.4 cm, fairly stationary up to meter level 109 (i.e., through the stratigraphic interval where mean sample spacing is ~5 cm). It is close to the peak with a period of 16.8 cm seen in the power spectra of the 1 cm sampled MS series (see Fig. 5A), possibly representing the tilt cycle. The weight percent $CaCO_3$ series bears an elevated frequency signal, although not quite reaching the 95% c.l., with a period of 37.9 cm, which may represent the dominant short eccentricity cycle in this time interval. This signal is most evident in the lower part of the section (5 cm sample spacing), somewhat mimicking the fuzzy short eccentricity signals seen in the more densely sampled MS series (Fig. 5A). However, the strong long eccentricity signal seen in the MS series with a period of 176 cm (Fig. 5A) is lacking in the weight percent $CaCO_3$ series (Fig. 5B). In the weight percent $CaCO_3$ series the most powerful frequency signal appears in the upper part of the section with a very long period wobbling around 10 m (i.e., ~2.2 m.y. frequency considering a mean sedimentation rate of 4.3 m m.y.$^{-1}$). Very long frequency signals appear also in the $\delta^{13}C$ and $\delta^{18}O$ series, but none shows any statistically significant signal in the long eccentricity frequency band, or even in the short eccentricity band, except perhaps for a brief, weak signal seen in the lower part of the section in the $\delta^{13}C$ series (Fig. 5D).

The results of the multiproxy cyclostratigraphic FFT spectral analysis described here indicate that the 1 cm sampled MS series yields the clearest and most statistically significant frequency signals, which are compatible with the predicted frequencies of the tilt and both short and long eccentricity. On the contrary, the $CaCO_3$, $\delta^{13}C$, and $\delta^{18}O$ series, with a mean sampling spacing of 5–10 cm, do not show any statistically significant frequency that could be confidently attributed to Milankovitch cycles. A closer look at the actual outcrop, and the multiproxy series superimposed on it, helps to illuminate the relation between sedimentation and bedding and the recording of environmental and climatic changes reflected by the variations in the multiproxy series (Fig. 6). As a first approach, the first meter of the Danian starting at the K-Pg boundary clay layer is framed in detail in Figure 6A. This basal Paleogene interval is the one that records the immediate aftermaths of the K-Pg boundary global environmental catastrophe following the Chicxulub extraterrestrial impact. The first impression one gets by looking at this K-Pg interval is the evident change in bedding style between the top of the Maastrichtian R2 member of the Scaglia Rossa Formation and the bottom of the Danian R3 member; in the former, stylolitic pseudobedding has a mean thickness of ~5–10 cm (as seen in the Bottaccione Gorge section shown in Fig. 4A), whereas in the basal R3 member, pseudobedding is much thinner, more like 3–7 cm, which gives the visual impression of a marly sediment. In reality, the $CaCO_3$ content through the first 60 cm of the R3 member is on average 94 wt% with a minimum of 92.5 wt% at 100.4 m level, while the rest of the entire Contessa Highway section has a mean $CaCO_3$ content of ~87 wt%, with minima of ~50–60 wt% in 8 distinct clay-rich layers in the interval between 101.9 and 103.4 m, an interval that include a biotite-rich volcanosedimentary layer at 01.99 m (the ALE volcanic ash in Odin et al., 1992; see also Fig. 2D). A narrow 4–9 cm bandpass filter of the 1 cm sampled MS series through the first meter of the Danian indicates that high MS values at such fine scale correspond to stylolite (clay) seams, i.e., pseudobedding (see Fig. 6A). In general, but not always, as seen at a sample to sample scale, low $CaCO_3$ corresponds to high MS (Fig. 6B), an expected relation that is more evident with a broader 36–63 cm bandpass filter (Fig. 6C). There are a few short stretches in the Contessa Highway section where this antiphase relation between $CaCO_3$ and MS is not valid.

Between the stable isotope $\delta^{13}C$ and $\delta^{18}O$ series, at a sample to sample scale it appears that in the first 20 cm of the Danian, high $\delta^{18}O$ corresponds to low $\delta^{13}C$, but then in the rest of this 1 m section the relation seems to be inverted (Fig. 6B). Nevertheless, a positive correlation between $\delta^{13}C$ and $\delta^{18}O$ is generally but not always seen through the rest of the Contessa Highway section, as highlighted by a 36–63 cm bandpass filter correlation in Figure 6C. However, in the terminal Maastrichtian Bottaccione Gorge section, the general relation between $\delta^{13}C$ and $\delta^{18}O$ is consistently antiphase (i.e., high $\delta^{18}O$ corresponds to low $\delta^{13}C$). Moreover, the 2 negative $\delta^{18}O$ excursions in the 100.4–100.6 m interval, that correspond to low excursions of the $\delta^{13}C$ proxy, and relatively high excursions of the MS proxy, are what characterizes the so-called DAN-C2, which was interpreted as an hyperthermal event possibly related to the aftermath of the K-Pg boundary global catastrophe (Coccioni et al., 2010, and references therein). There is a general positive relation between the $\delta^{18}O$ and the MS series through the entire Contessa Highway section, as highlighted by a 36–63 cm bandpass filter correlation in Figure 6C. The same

relation is seen in the terminal Maastrichtian Bottaccione Gorge section (Fig. 4C).

The cyclostratigraphic analysis of the Contessa Highway section based on multiproxy series highlights some sedimentological problems in the basal 1 m of the Danian. The stationarity and power of the long and short eccentricity and tilt signals from the MS and $CaCO_3$ series suggest a mean sedimentation rate of 4.3 m m.y.$^{-1}$ throughout the 14-m-thick section (Figs. 4A, 4B), which agrees with the geochronology of the Danian in the Gubbio succession by Coccioni et al. (2012b). However, high-resolution analysis of ^{3}He across the K-Pg interval in the Bottaccione Gorge section by Mukhopadhyay et al. (2001), i.e., the component of perennial interplanetary dust particles fallout, suggests a ~10 m m.y.$^{-1}$ sedimentation rate for the basal 40 cm of the Danian (the so-called Eugubina limestone, i.e., the indistinct P0-Pα Zones), a rate that is close to a mean sedimentation rate of the terminal Maastrichtian (see Fig. 7). A mean ^{3}He concentration of 60 × 10^{-15} cm^3 g^{-1} is the same in the top of the R2 member of the Scaglia Rossa as in the Eugubina limestone; the concentration of the noncarbonate terrigenous component of ~5 wt% (i.e., 95 wt% $CaCO_3$) in these limestones across the K-Pg boundary is also the same (Fig. 7). Nevertheless, at Contessa Highway the 1 cm sampled MS series and the 5 cm sampled $\delta^{18}O$ series show broad compositional variations defining 2 cycles with a wavelength of ~16 cm (see dashed lines in Fig. 6B), possibly representing the precession cycle (i.e., a period of ~20 k.y.). This would imply a mean sedimentation rate of ~8 m m.y.$^{-1}$, thus a duration of ~50 k.y. of the ~40-cm-thick P0-Pα Zones. In the 60 cm interval immediately above the Eugubina limestone, the ^{3}He concentration rises to a mean of ~140 × 10^{-15} cm^3 g^{-1}, i.e., a factor of 2.2 higher than in the Eugubina limestone, whereas the biogenic $CaCO_3$ concentration drops to a mean of ~84 wt%, much lower than a mean of 95 wt% in the underlying Eugubina limestone (Fig. 7). All this suggests that this 60 cm marly limestone interval has a sedimentation rate lower than 8 or 10 m m.y.$^{-1}$ estimated for the underlying K-Pg limestones from the ^{3}He record and may represent a condensed interval, probably reflecting the paleoclimatic hyperthermal event known as the Dan-C2 (see Coccioni et al., 2010, and references therein). Above this Dan-C2 interval, the ^{3}He concentration drops to a mean of ~90 × 10^{-15} cm^3 g^{-1} (Fig. 7), lower than the mean concentration of 60 × 10^{-15} cm^3 g^{-1} measured in the terminal Maastrichtian R2 limestone and the basal Danian

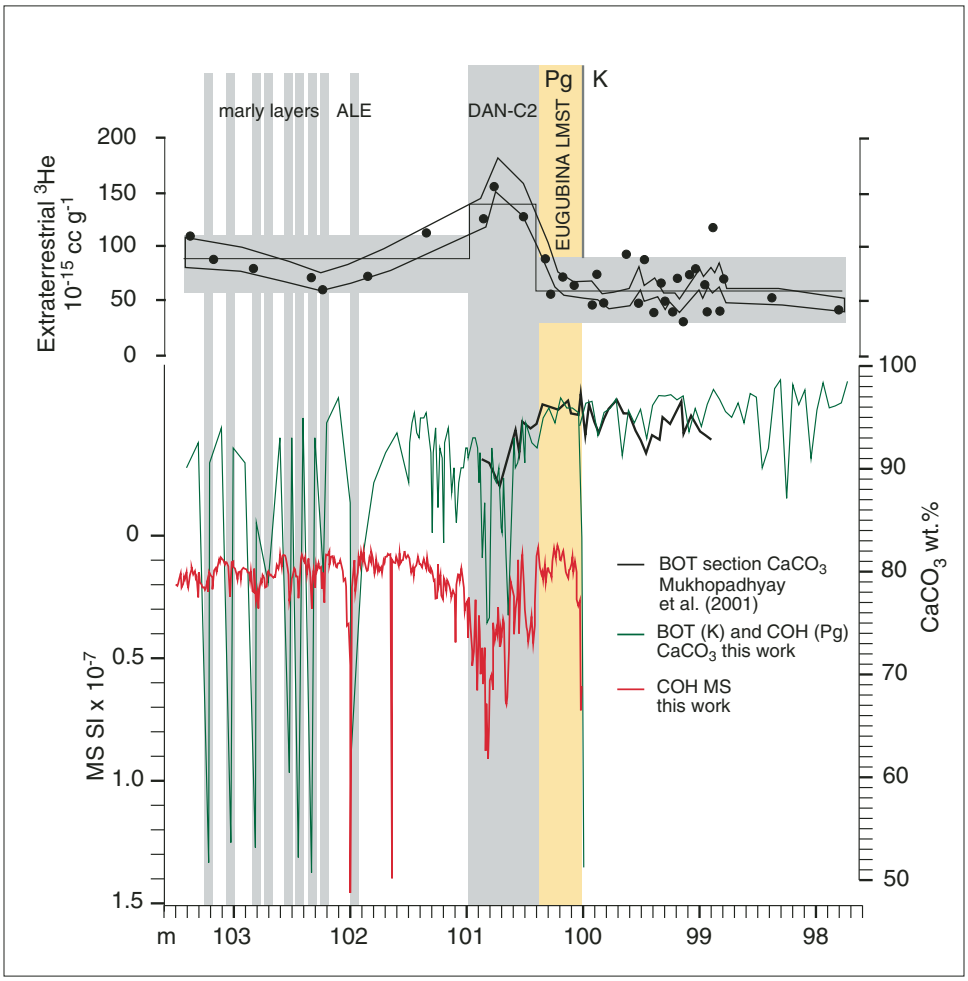

Figure 7. The extraterrestrial ^{3}He record across the Cretaceous-Paleogene (K-Pg) boundary in the Bottaccione section (BOT) from Mukhopadhyay et al. (2001) compared with the magnetic susceptibility (MS) and $CaCO_3$ data series from the same stratigraphic interval in the Contessa Highway section (COH; see text for detailed explanation). LMST—limestone.

Eugubina limestone measured by Mukhopadhyay et al. (2001) that may indicate a mean sedimentation rate lower than 8–10 m m.y.$^{-1}$ estimated for the underlying narrow K-Pg boundary interval. In this interval, other than the thin ALE biotite-rich volcaniclastic layer, between meter levels 102.1 and 103.4 (130 cm interval) there are 8 distinct, thin marly horizons (i.e., with $CaCO_3$ compositions ranging between 52 and 62 wt%; see Fig. 7), thus with a mean period of 16.3 cm. This period is very close to the period of 16.8 cm of the sharp and stationary frequency peak seen in the FFT spectra for the MS proxy series (Fig. 5A), and fairly close to a less sharp and stationary peak with a mean period of 17.4 cm revealed by the FFT spectra for the $CaCO_3$ proxy series (Fig. 5B). This frequency peak would correspond to a period of ~39 k.y. by applying a mean sedimentation rate of 4.3 m m.y.$^{-1}$ to the entire 14-m-thick Contessa Highway section, and should be the expression of the tilt (obliquity) cycle as predicted by Laskar et al. (2004).

PALEOCLIMATE INTERPRETATIONS

The MS intensity and weight percent $CaCO_3$ proxy records can be interpreted interchangeably, because they are inverse proxies that respond to the same environmental signal, i.e., the ratio of carbonate to terrigenous material in the sediment. The weight percent $CaCO_3$ depends on the amount of the biogenic calcareous material, mostly represented by calcareous nannoplankton and planktonic foraminifera, that reaches and is preserved on the seafloor. The terrigenous material measured by the MS intensity signal was transported to the Umbria-Marche paleobasin by wind, river runoff, or a combination of both. According to the paleogeographical reconstructions (Dercourt et al., 1993; Rosenbaum et al., 2002; Adatte et al., 2002), the paleogeography of the Gubbio sections was a deep marine basin a few hundred kilometers away from subtropical and/or tropical shallow-water carbonate platforms (Fig. 1B), while continental landmasses like Europe and Asia to the north and northeast and Africa to the south were more than 500 km away (Figs. 1B and 8). At such distances, most of the runoff suspension probably settled before reaching the Umbria-Marche Basin. Therefore, the input of terrigenous material from a fluvial source in the Late Cretaceous–early Paleogene Umbria-Marche pelagic basin can be excluded. We deduce that the MS signal imparted by the terrigenous component in the Scaglia Rossa pelagic limestones is mainly eolian in origin, as proposed by Arthur and Fischer (1977) and Johnsson and Reynolds (1986).

The eolian dust was probably mainly produced in desert lands, where the lack of vegetation would have favored its mobilization. Based on modeled vegetation cover for the Maastrichtian, two desert or semidesert regions may be considered as possible sources for the eolian dust (e.g., Upchurch et al., 1999; Hunter et al., 2013). The first region was located to the southwest of the Umbria-Marche Basin, and corresponds to the northwestern corner of Africa (Fig. 8, i.e., the modern subtropical Atlas region), which, according to paleogeographic reconstructions (e.g., Dercourt et al., 1993; Hay et al., 1999) was between lat 10°N and 20°N in the Late Cretaceous. The second possible arid source region was a much larger South Asia area, the Cretaceous Asian zone (Fig. 8), roughly comprising the modern regions of Kazakhstan and Mongolia, which in the Late Cretaceous were between 30°N and 40°N, bordering the tropical eastern Tethys Ocean. Today, the northeast trade winds dominate the general atmospheric circulation above North Africa. Winds and associated dust transport vary through the year with the Intertropical Convergence Zone (ITCZ) (Prospero et al., 1981). During the Northern Hemisphere (NH) summer, the trade winds are more constrained and the high temperatures over the Sahara create strong surface winds and convection cells (Pey et al., 2013). The convection lifts dust particles and transports them at higher atmospheric levels. Although the bulk of dust from the modern Sahara Desert and the Sahel is deposited west of the continent (i.e., in the tropical Atlantic), a fraction is transported toward the Mediterranean (Pey et al., 2013). The Africa-Eurasia continental distribution in the Cretaceous was different than the current geographic setting, but similar processes could have been active. Today, the winter high-pressure zone above the continent of Asia results in winds going from the northeast to the southwest along the southern borders of the continent. During the Cretaceous, a similar high-pressure zone could have developed above the large Asia landmass, resulting in winds transporting dust from the large bare areas on this continent toward the western Tethys. A coupled atmosphere-ocean general circulation model (GCM) for the Late Cretaceous indicates the presence of an Asian monsoon system, although it was weaker than the present-day system (Bush and Philander, 1997); the same study indicates that monsoon-related precipitation rates for northwestern Africa were comparable to present-day values.

The MS and weight percent $CaCO_3$ proxy series of the latest Maastrichtian Bottaccione Gorge section yielded power spectra with peaks in the frequency bands of the precession and obliquity (Figs. 4A, 4B). As evident from the evolutionary FFTs (Figs. 4A, 4B), the lower half of the Bottaccione Gorge section is dominated by obliquity, while the upper part is dominated by precession. There is a short eccentricity signal, in combination with precession, visible in the MS power spectrum, while it is seemingly absent or very weak in the weight percent $CaCO_3$ power spectrum; this is probably the result of differences in the data quality of those proxies (see Materials and Methods discussion). From these observations, two questions arise, i.e., what mechanisms are responsible for the frequencies in our records, and what represents the shift from an obliquity-dominated toward a precession-dominated spectrum of the MS series (Fig. 4A) in the middle of the studied interval.

The evolution of insolation at 25°N (estimated paleolatitude of Gubbio) over time is dominated by precession (Fig. 8). The position of the ITCZ and the strength of the monsoon systems respond to changes in insolation (e.g., Prospero et al., 1981; Tuenter et al., 2003, 2005). Along with the expected precessional component in the modern African monsoon system, a

pronounced obliquity component is often observed (e.g., Tuenter et al., 2003, and references therein). The obliquity component is at first unexpected, as the largest obliquity insolation amplitude effect is found at higher latitudes. However, the Earth's climatic system is interconnected between the latitudes and there is potential for interplay between high and low latitudes (e.g., oceanic and atmospheric currents, Tuenter et al., 2003, 2005). Moreover, Tuenter et al. (2003) indicated that these remote mechanisms have the most significant influence in the subtropics (20°–30°N). Tuenter et al. (2005) found that stronger monsoons occurred during maximum obliquity and vice versa. A GCM study performed on settings of the mid-Cretaceous found a significant obliquity signal in the hydrological cycle over proto–West Africa (Park and Oglesby, 1991).

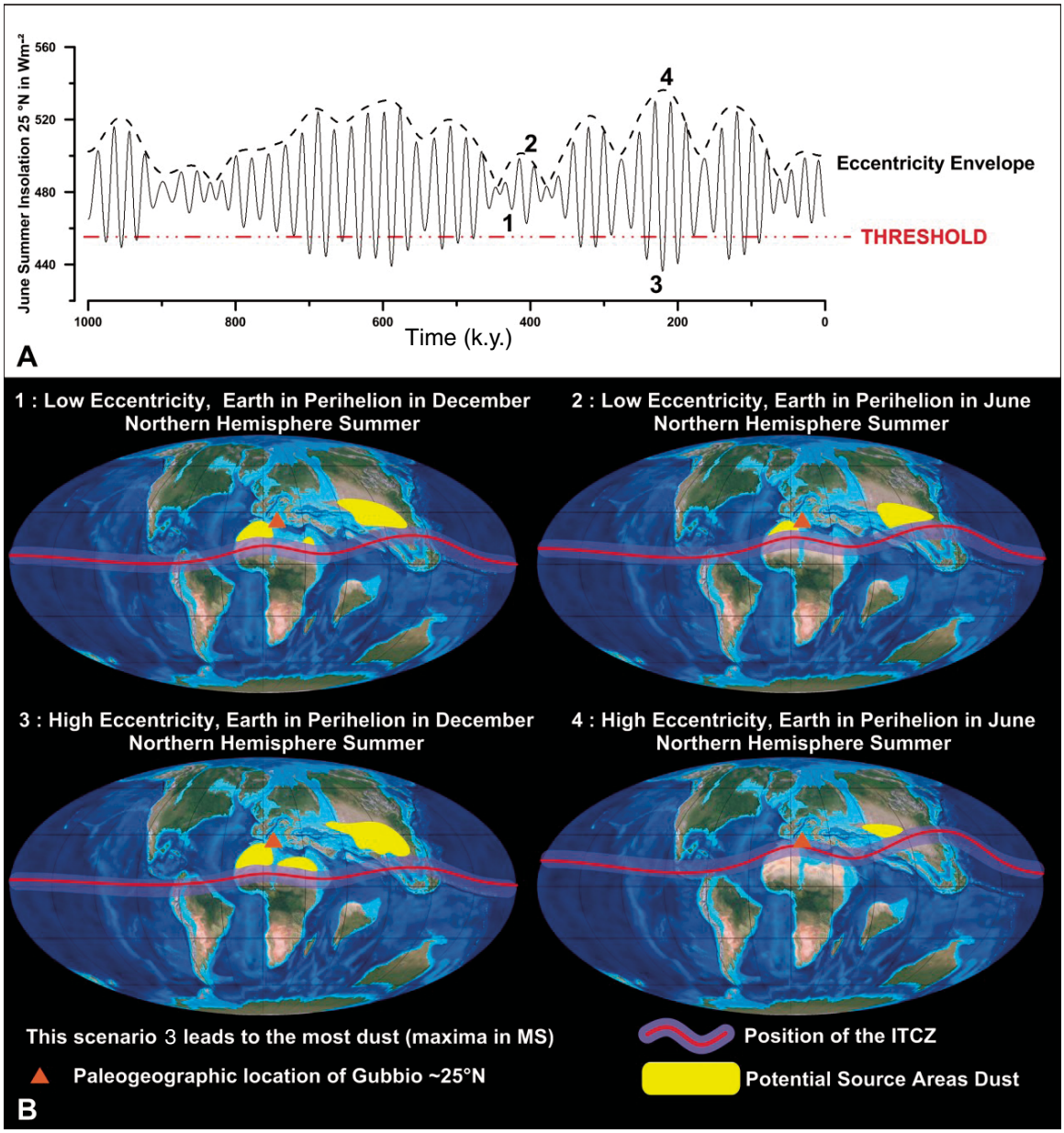

Figure 8. Schematic illustration of the proposed threshold mechanism. (A) June insolation for 25°N, dominated by eccentricity-modulated precession (Laskar et al., 2004). (B) When Northern Hemisphere summer insolation is lower than an arbitrary chosen threshold, the Intertropical Convergence Zone (ITCZ) doesn't reach as far north as compared to a higher Northern Hemisphere summer insolation. Subtropical drought is triggered and the vegetation cover declines dramatically in the areas indicated in yellow (i.e., a nonlinear vegetation response). The potential for dust transportation (reflected by peak magnetic susceptibility in the Gubbio section) is thus highest in scenario 3. Paleogeographical reconstructions by Ron Blakey.

All these models do not include ice sheet components to explain the effect of high-latitude insolation on low-latitude climatology; it is unlikely that large permanent ice sheets existed at the end of the Cretaceous. Nevertheless, there are indications of the presence of significant terrestrial ice volumes present during that period in polar regions (e.g., Miller et al., 2005; Price and Nunn, 2010). One of the significant peaks in the $\delta^{18}O$ spectral plot (Fig. 4C) is at ~43 k.y. Changes in obliquity must have influenced this glacial climatic component and the latitudinal temperature gradient. Therefore, the patterns in the exchange of energy (oceanic and atmospheric currents) would have changed, resulting in climatic changes at lower latitudes also. These processes could explain why the lithological proxies show a prominent obliquity signal in the lower part of the Bottaccione Gorge section. The transition from obliquity-dominated to precession-dominated spectra occurs in the same interval as the shift in the $\delta^{18}O$ record (~4 m below the K-Pg boundary), which could be associated with global warming induced by the Deccan volcanism (Fig. 9). A global warming would imply that the latitudinal temperature differences become smaller and that the climate zones shift more toward the poles. The position of the ITCZ during the solstices could have been shifted away further from the equator than compared to a global cooler climatic setting. It follows that the paleolocation of Gubbio came under the influence of a purely tropical climatic regime, dominated by precession, whereas its earlier situation was characterized by a subtropical regime in which remote (obliquity) mechanisms have a larger effect. The warming probably triggered the melting of the land ice masses, reducing the potential for ice-related feedbacks, and thereby limiting the potential of transferring obliquity-related climate variability from high to low latitudes.

The spectral peak in the eccentricity band (Fig. 4A) requires further discussion, as eccentricity does not directly influence the amount of incoming solar radiation; therefore, we propose a threshold mechanism to explain its observation. The position of the ITCZ and intensity of the modern African and Asian monsoon systems are influenced by changes in insolation (Fig. 8). Therefore, the same principal arguments may be followed and applied to the Cretaceous Tethyan-Asian context. Today, a stronger African monsoon would result in a "greener Sahara-like" environment, i.e., an expansion of savannah-like vegetation and an increase of soil moisture would stimulate soil coherence and thus decrease the production and export of dust. Moreover, once vegetation is established, feedback mechanisms can further enhance the development of vegetation; e.g., a darker albedo and the establishment of primary vegetation increases water-retaining capacity. A stronger African monsoon occurs when the Northern Hemisphere summer occurs near the perihelion, resulting in a stronger insolation (defined as minimum precession) and vice versa (Fig. 8). These dynamics and the effects of vegetation and its feedbacks are well studied for the green Sahara period during the Holocene, which occurred at a precession minimum (i.e., Northern Hemisphere summer insolation maximum; e.g., Kutzbach, 1981; Claussen, 1997; Kutzbach and Liu, 1997; Ganopolski et al., 1998; Kröpelin et al., 2008). The amplitude of the precession is modulated by eccentricity; therefore seasonal contrasts are both enhanced and dampened during eccentricity maxima. During eccentricity minima, seasonal extremes are avoided for a prolonged period of time. On the basis of these observations, we propose a threshold mechanism related to the latitudinal extent of the ITCZ dynamics (Fig. 8). Under a pronounced precession maximum (i.e., Northern Hemisphere summer insolation minimum) during high eccentricity, monsoonal circulation is so weak and does not extend far enough north that it cannot sustain a minimum of vegetation cover (Fig. 8). When this threshold is exceeded, large landmasses lose their vegetation because of the extreme periods of drought and thus become source areas for eolian dust. Through dynamics of savannah-type vegetation (grasses, Hunter et al., 2013), a large area on the northwest African continent is susceptible to responding to this threshold mechanism. The increase of dust transport would lead to an increase of the terrigenous fraction in marine deep-water sediments and would consequently result in a peak in MS (Fig. 3B). During eccentricity minima, these variations would be less pronounced and the thresholds would not be exceeded.

We observe only 405 and 100 k.y. variations in the $\delta^{13}C$, in agreement with numerous published records (e.g., Cramer et al., 2003; Pälike et al., 2006; Russon et al., 2010; Zachos et al., 2010; Batenburg et al., 2012, and references therein). The increase in dust particles toward modern Mediterranean means an augmentation in nutrients for primary producers. The model of Russon et al. (2010) demonstrates that relatively small variations in the relative and total amount of nutrients in the global oceans could account for a 400–500 k.y. $\delta^{13}C_{DIC}$ (dissolved inorganic carbon) periodicity. Boosts in primary production result in lower $\delta^{13}C$ values as the so-called rain ratio is changed: the ratio between the export of organic carbon ($\delta^{13}C \sim -29‰$) and the export of marine biogenic calcium carbonate ($\delta^{13}C \sim 0‰$). During eccentricity minima, seasonal extremes are avoided for longer times; these boosts in primary production will be less likely to occur and thus primary production will vary around a mean rate. During eccentricity maxima, periods of high and low seasonality alternate, but at the times of high seasonality the increases in primary production at certain times will gradually cause a decrease in the $\delta^{13}C$ record as the production of organic carbon is stimulated by the input of more nutrients. At eccentricity minima, boosts in primary production will occur less often and the carbon record will have more time to become positive. It is possible that the long

Figure 9. The $^{187}Os/^{188}Os$ record of the terminal Maastrichtian in the Bottaccione section from Robinson et al. (2009), plotted against the four proxy data series from this work, with interpretative annotations of environmental and paleoclimatic events (see text for detailed explanation). The lower meter scale refers to the stratimetry of the Gubbio Albian to Maastrichtian calcareous plankton biostratigraphy and magnetostratigraphy of Coccioni and Premoli Silva (2015). Pg—Paleogene; K—Cretaceous.

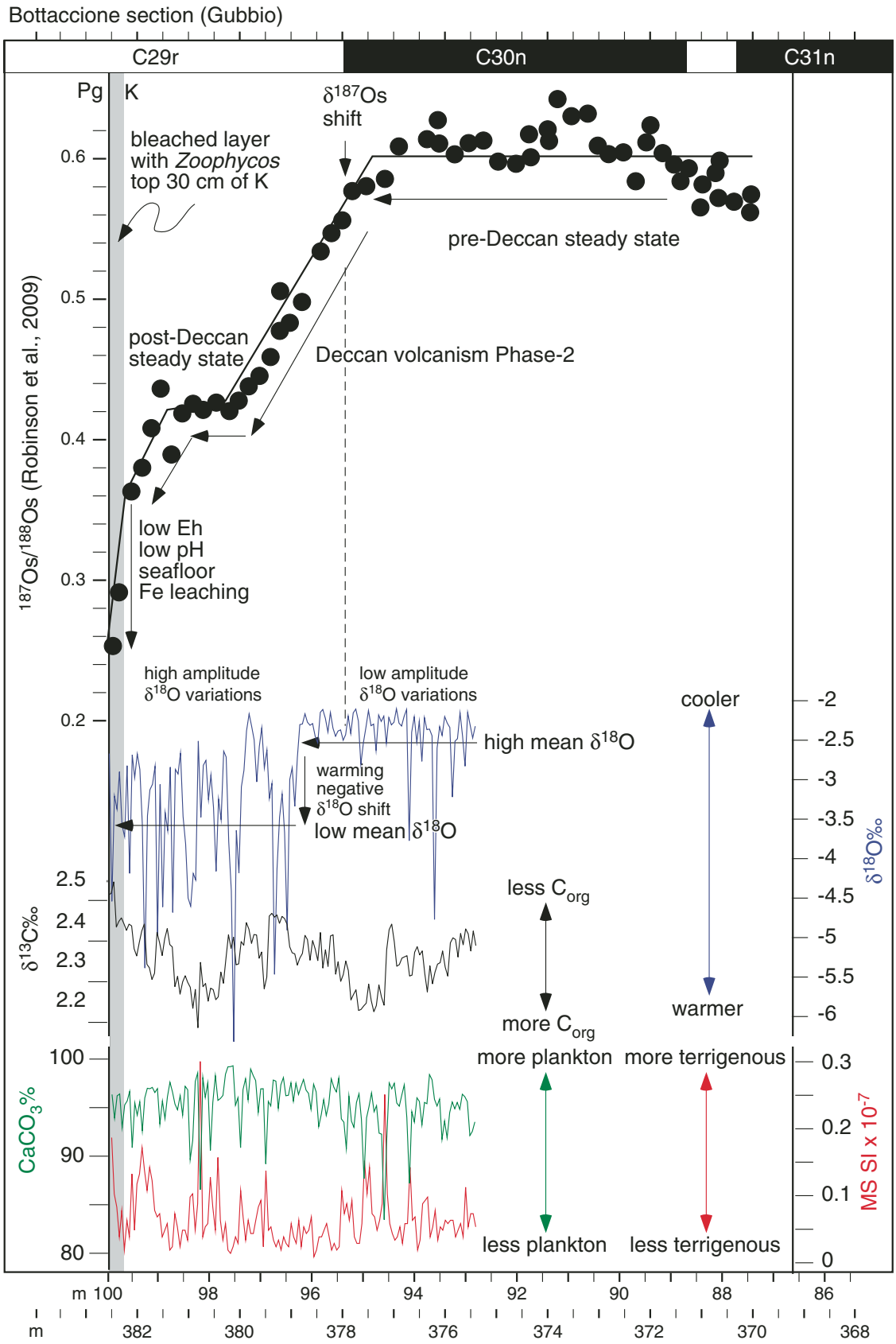
Bottaccione section (Gubbio)
C29r
C30n
C31n
Pg
K
δ187Os shift
bleached layer with Zoophycos top 30 cm of K
pre-Deccan steady state
post-Deccan steady state
Deccan volcanism Phase-2
low Eh
low pH
seafloor
Fe leaching
187Os/188Os (Robinson et al., 2009)
high amplitude δ18O variations
low amplitude δ18O variations
high mean δ18O
warming
negative
δ18O shift
low mean δ18O
cooler
warmer
δ18O‰
δ13C‰
less Corg
more Corg
more plankton
more terrigenous
less plankton
less terrigenous
CaCO3%
MS SI x 10-7
m
m 100
98
96
94
92
90
88
86
382
380
378
376
374
372
370
368

Figure 9.

residence time of carbon in the ocean (~10^5 yr) amplifies longer (astronomical) forcing periods (Cramer et al., 2003; Pälike et al., 2006), explaining the observed eccentricity signal and the lack of a precessional signal (Fig. 4D).

Zachos et al. (2010) suggested another paleoclimatological mechanism that explains the amplification of the eccentricity cycles. This paper focuses on primary production in the marine environment, while they proposed a prominent role for land-based organic carbon reservoirs. Both mechanisms are not mutually exclusive. It is useful to evoke the elements of a threshold and the long residence time of carbon in the ocean. The environmental conditions have to be dry and prolonged enough that wetlands cannot be sustained. As a result of this, large quantities of organic carbon can be transported toward the oceans, leading to lower $\delta^{13}C$ values in the record. Through this climatic link, variation in the carbon cycle, including negative excursions as K-PgE1 and K-PgE3, can be linked to astronomical forcing (see Batenburg et al., 2012; Voigt et al., 2012) as well as to volcanic activity (Husson et al., 2014).

In summary, these interpretations suggest a phase relationship between high eccentricity and lower $\delta^{13}C$ and MS maxima ($\approx CaCO_3$ minima), and vice versa.

The paleogeographic and geologic-tectonic settings of the Tethyan domain in the latest Cretaceous was presumably the same as in the earliest Paleogene. However, what may have changed drastically were the paleoenvironmental and climatological conditions following the K-Pg boundary impact–induced global catastrophe. The high-resolution MS series from the Danian Contessa Highway section yielded power spectra similar to those of the latest Cretaceous Bottaccione Gorge section, with pronounced and fairly stationary obliquity and eccentricity signals (Fig. 5A), but the sedimentation rate dropped significantly from a mean of 10.7 m m.y.$^{-1}$ in the Cretaceous to 4.3 m m.y.$^{-1}$ through the Danian. Moreover, the 1 m interval immediately above the K-Pg boundary clay layer has anomalous sedimentary records such as the 40-cm-thick porcelain-like Eugubina limestone, which may represent a sedimentation rate of ~9 m m.y.$^{-1}$, and the subsequent 60-cm-thick marly interval manifesting the Dan-C2 hyperthermal event (Coccioni et al., 2010, and references therein), which may represent sedimentary condensation (see Fig. 7). Apart from these sedimentological anomalies, which may reflect a period of climatic and environmental instability in the immediate aftermath of the K-Pg boundary catastrophe, sedimentation through the rest of the Danian seems to have responded to the same paleoclimatological forcings that were acting in the latest Cretaceous. Nevertheless, a generally lower $CaCO_3$ content and higher MS with respect to the Cretaceous section up to meter level 110 (see Fig. 2D) suggest that environmental conditions in the eolian dust source areas changed after the K-Pg boundary catastrophe for ~2.5 m.y. These interpretations suggest a concordant phase relationship between high eccentricity and MS maxima for the Danian Contessa Highway section and the latest Cretaceous Bottaccione Gorge section.

ASTROCHRONOLOGIC TUNING AND DATING OF BIOMAGNETOSTRATIGRAPHIC EVENTS ACROSS THE TERMINAL MAASTRICHTIAN AND DANIAN

The MS proxy series for both the uppermost 7.2 m of the Maastrichtian in the Bottaccione section (sampling spacing of 5 cm), and the entire 14-m-thick Danian section along the Contessa Highway (sampling spacing of 1–2 cm) best serve the purpose of identifying cyclic variations in sedimentation through this ~4.5–m.y.-long continuous and complete stratigraphic record across the K-Pg boundary. Our cyclostratigraphic analysis using FFT revealed that frequency signals corresponding to long and short eccentricity cycles and tilt are statistically significant on a 95% c.l., and fairly stationary throughout this Bottaccione–Contessa Highway section composite section (Figs. 3A and 5A). In our opinion, attempts to define Milankovitch cycles through the very same Bottaccione Gorge section and the lower 6.5 m of the Contessa Highway section by Husson et al. (2014), fell short in recognizing statistically meaningful frequencies in the bands of ~100 k.y. (short eccentricity) and ~40 k.y. (tilt) because of the too low resolution sampling of ~6 cm. The relative stationarity of the frequency signal with a period of 40.6 cm in our Bottaccione Gorge section, and 16.8 cm in the Contessa Highway, not only suggests relatively constant sedimentation rates in the respective separate stratigraphic intervals, but also enables us to derive precise mean sedimentation rates for the two sections by assuming a tilt period of ~39 k.y. (Laskar et al., 2004). In this way we obtain a mean sedimentation rate of 10.7 m m.y.$^{-1}$ for the Bottaccione Gorge section, and 4.3 m m.y.$^{-1}$ for the Contessa Highway section, notwithstanding that small changes in sedimentation rate may be present through these sections, as we inferred for the basal 1 m interval of the Danian at Contessa Highway (see Fig. 7).

Once the cyclic characters of the terminal Maastrichtian R2 member and the Danian R3 member of the Scaglia Rossa pelagic limestone have been confidently defined by spectral analysis of the high resolution MS series, an attempt can be made to tune the entire cyclic record to that of Laskar et al. (2011). This was done using a bandpass filter curve for both long and short eccentricity frequency bands matched to the eccentricity calculated by the astronomical solution. The filter band width of 85–150 cm for the Bottaccione Gorge MS proxy series is large enough to encompass the short eccentricity signal given a mean sedimentation rate of 10.7 m m.y.$^{-1}$, and presuming possible small variations in sedimentation rate around such mean value, but narrow enough to filter out possible noisy frequency signals. The same eccentricity signal can be extracted from the MS series of the Danian Contessa Highway section using a filter of 37–65 cm. Similarly, bandpass curves with broader filters of 285–500 cm for the Bottaccione Gorge section and 129–216 cm for the Contessa Highway section represent the long eccentricity cycle, i.e., its low-frequency modulation of ~406 k.y., which emerged from the FFT outputs in Figures 3A and 5A. We use this low-frequency bandpass curve for tuning the entire Bottaccione–Contessa

Highway stratigraphic section to the equivalent long eccentricity signal obtained from the eccentricity calculated by Laskar et al. (2011) by applying a bandpass filter of 300–500 k.y. (Fig. 10B). However, in order to perform such a tuning operation correctly, a phase relation has to be established between the stratigraphic record and the actual calculated short and long eccentricity record. As explained in detail in the Paleoclimate Interpretations section, we chose a concordant phase relationship between high eccentricity and MS maxima for both the Maastrichtian Bottaccione Gorge and the Danian Contessa Highway sections.

Another requirement for our tuning attempt is the definition of the numerical age for the K-Pg boundary, which has to be anchored to the geochronologic age of 66.0 ± 0.1 Ma assigned to it in the most recent geologic time scale by Gradstein et al. (2012, and references therein). The astrochronologic age of 66 Ma in the solution of Laskar et al. (2011) is near a maximum in the short eccentricity cycle, and near a minimum in the long eccentricity cycle. In our Gubbio composite section, the K-Pg boundary happens to be near a minimum in the long eccentricity cycle, as defined by a 285–500 cm bandpass filter curve (Fig. 10B), thus concordant with the solution of Laskar et al. (2011).

In Figure 10B, we show how astrochronologic ages for magnetozone boundaries are derived from the tuning of the Bottaccione–Contessa Highway composite section to the long eccentricity cycle of Laskar et al. (2011). In the same way, astrochronologic ages for calcareous nannofossil and planktonic foraminifera biozone boundaries are obtained and reported in Table 1 (also shown in Fig. 2C). In addition to a deep understanding of the sedimentology and paleoclimatology of the Scaglia Rossa and its paleoecological response to the K-Pg boundary impact, this new astrochronology provides a precise temporal framework for the biomagnetostratigraphic interval. Imprecise determination of the stratigraphic positions (meter level) of the C28n-C27r and C27r-C28n boundaries in the magnetostratigraphy of Lowrie et al. (1982) make comparison of the durations of these magnetozones with previous results challenging. In general, our astrochronological framework is in close agreement with that proposed by Dinarès-Turell et al. (2014).

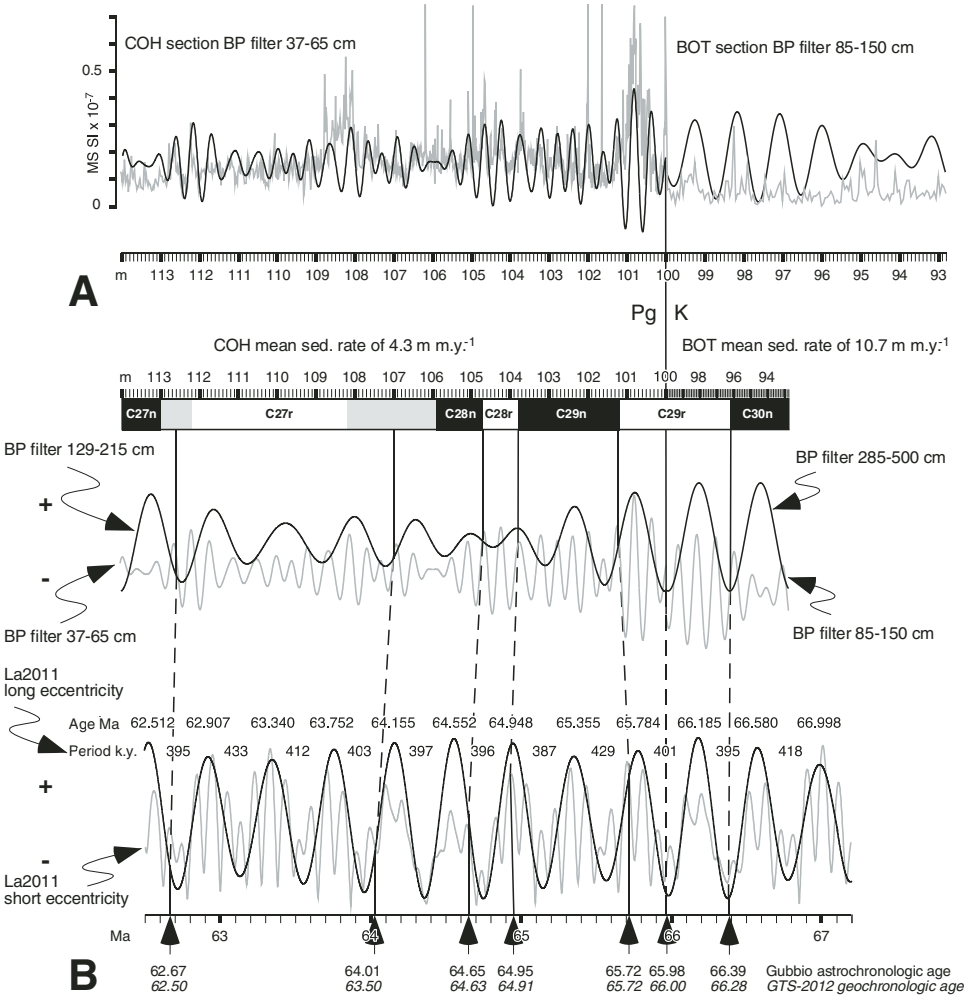

Figure 10. (A) High-resolution magnetic susceptibility (MS) data series of the entire composite Bottaccione–Contessa Highway (BOT-COH) Cretaceous–Paleogene (K-Pg) section; the relative bandpass (BP) curves filtered for the short eccentricity cycle are superimposed. (B) Tuning with the long and short eccentricity cycles from the nominal solution of Laskar et al. (2011; La2011) of the BOT-COH composite biomagnetostratigraphic section based on the high-resolution MS series BP filtered for the eccentricity cycle. GTS-2012 is geologic time scale of Gradstein et al. (2012); sed—sedimentation.

TABLE 1. ASTROCHRONOLOGICAL AGE DETERMINATION OF BIOSTRATIGRAPHIC AND MAGNETOSTRATIGRAPHIC EVENTS ACROSS THE CRETACEOUS–PALEOGENE BOUNDARY IN THE BOTTACCIONE-CONTESSA HIGHWAY COMPOSITE SECTION OF GUBBIO COMPARED TO GEOCHRONOLOGIC AGES

Biostratigraphic and magnetozone boundary	BOT-COH m level	Geochronological age (Ma) GTS-2012	Astrochronological age (Ma) Gubbio*	Stratigraphic age error (m.y.) Gubbio†
C27n-C27r	112.60	62.50	62.672	± 0.100
P3a-P2	112.45	62.28	62.711	± 0.005
P2-P1c	109.75	62.60	63.349	± 0.005
Ellipsolithus macellus-Cruciplacolithus tenuis	107.75		63.820	± 0.005
Ellipsolithus macellus-Cruciplacolithus edwardsii	107.75		63.820	± 0.005
NP4-NP3	107.75	63.22	63.820	± 0.005
CP3-CP2	107.75	63.22	63.820	± 0.005
C27r-C28n	107.00	63.50	64.012	± 0.280
P1c-P1b	105.35	63.89	64.457	± 0.005
NP3-NP2	104.85	64.80	64.622	± 0.005
CP2-CP1b	104.85	64.80	64.622	± 0.005
C28n-C28r	104.80	64.63	64.553	± 0.010
Cruciplacolithus tenuis-Prinsius dimorphosus	104.25		64.810	± 0.005
C28r-C29n	103.80	64.91	64.952	± 0.010
Prinsius dimorphosus-Cruciplacolithus primus	102.75		65.228	± 0.005
P1b-P1a	102.25	65.21	65.358	± 0.005
Cruciplacolithus edwardsii-Cruciplacolithus primus	101.95		65.455	± 0.005
NP2-NP1	101.35	65.45	65.603	± 0.005
CP1b-CP1a	101.35		65.603	± 0.005
C29n-C29r	101.20	65.70	65.720	± 0.050
Cruciplacolithus primus-Biantholithus sparsus	100.75		65.880§	± 0.005
P1a-P0-Pα	100.55	65.70	65.923§	± 0.005
K-Pg boundary	100.00	66.00	65.984	± 0.005
K-Pg boundary	100.00	66.043±0.043#	65.984	± 0.005
K-Pg boundary	100.00	66.0387±0.025/0.039**	65.984	± 0.006
P0-Pα-*Plummerita hantkeninoides*	100.00		65.984	± 0.005
NP1-NC23	100.00		65.984	± 0.005
CP1a-CC26b	100.00		65.984	± 0.005
Biantholithus sparsus-UC20d	100.00		65.984	± 0.005
Biantholithus sparsus-Micula murus-Micula prinsi	100.00		65.984	± 0.005
Plummerita hantkeninoides-Pseudotextularia elegans	98.59		66.139	± 0.005
CC26b-CC26a	96.50		66.355	± 0.025
UC20d-UC20b-c	96.50	66.33	66.355	± 0.025
C29r-C30n	96.20	66.28	66.390	± 0.025
Pseudotextularia elegans-Pseudoguembelina hariaensis	95.17		66.503	± 0.005

Note: K-Pg—Cretaceous-Paleogene; BOT-COH—Bottaccione-Contessa Highway. Geochronologic ages as in the geological time scale of Gradstein et al. (2012). Gray—magnetic polarity chron; blue—planktonic foraminiferal zone; green—calcareous nannofossil zone.

*The astrochronolochronologic ages are derived from the tuning of the long eccentricity filtered curve of the MS series for the composite BOT-COH section with the long eccentricity of Laskar et al. (2011), as shown in Figure 10 (see text).

†The error of the astrochronologic ages is derived from the sampling spacing in the sections analyzed by: Roggenthen and Napoleone (1977) for the BOT magnetostratigraphy; Lowrie et al. (1982), in part amended by Coccioni et al. (2010) for the COH magnetostratigraphy; Coccioni and Premoli Silva (2015) for the BOT planktonic foraminifera; Coccioni et al. (2012b) for the COH planktonic foraminifera and COH calcareous nannofossils; Gardin et al. (2012) for the BOT calcareous nannofossils; and Coccioni et al. (2012b) for the COH calcareous nannofossils.

§Ages corrected considering a sedimentation rate for the basal 60 cm of the Danian of 9 m m.y.$^{-1}$ (see text for explanation).

#Preferred absolute age for the K-PgB by Renne et al. (2013) with 1s error.

**Combined Ar/Ar age for the Beloc (Haiti) tektites by Renne et al. (2013) with 1s error.

Galeotti et al. (2015) constructed a cyclostratigraphic framework based on a high-resolution weight percent $CaCO_3$ record for the Danian in the Bottaccione Gorge; their results differ from our conclusions in identifying an additional long eccentricity cycle in the magnetochron C29n. This stratigraphic interval is sedimentologically challenging to interpret (see the discussion of the Contessa Highway section herein and Fig. 7); however, we conclude that the new high-resolution MS series is the most suitable to identify the eccentricity cycles. Moreover, there are slump structures in this interval at the Bottaccione section, which motivated the use of the Bottaccione–Contessa Highway composite in this study.

CONCLUSIONS

We studied the paleoclimate of the latest Maastrichtian and earliest Paleogene, based on a high-resolution multiproxy data set consisting of MS, weight percent $CaCO_3$, and oxygen and carbon stable isotopes. The signal from the MS series is interpreted to reflect variations in the eolian influx into the Umbria-Marche Basin. We propose a relationship between paleoclimatological and paleoenvironmental settings and astronomical parameters to account for the wind-blown terrigenous influx variations, which suggest a vegetation cover threshold mechanism as responsible for the observed eccentricity periodicity in the MS. It is possible that the $\delta^{18}O$ record was affected by a warming induced by the Deccan-2 volcanic stage, starting ~400 k.y. prior to the K-Pg boundary. Global warming could have caused a poleward shift of the climatic zones and could therefore explain the dominance of the obliquity signal in the lower half of the terminal Maastrichtian Bottaccione Gorge section, whereas precession controls the upper half.

These interpretations suggest a phase relationship between high eccentricity and lower $\delta^{13}C$ and MS maxima ($\approx CaCO_3$ minima), and vice versa; based on these phase relationships, an astronomical tuning of the Contessa Highway and Bottaccione Gorge sections is presented. Table 1 reports the estimated timing and duration of several biostratigraphic and magnetostratigraphic events in both sections.

ACKNOWLEDGMENTS

This research has been funded by the Interuniversity Attraction Poles Program (Planet Topers) initiated by the Belgian Science Policy Office, and supported by the Associazione Le Montagne di San Francesco in Coldigioco, Italy. Matthias Sinnesael was supported by the Vrije Universiteit Brussel research fund; he thanks Linda Hinnov for a fruitful discussion concerning the tuning of the Contessa Highway Danian section. Claeys thanks the Hercules Foundation for the upgrade of the stable isotope lab and support, and the Research Foundation Flanders (grant G0B8513N). Luigi Jovane is supported by FAPESP (Fundação de Amparo à Pesquisa do Estado de São Paulo, processo JP 2011/22018-3) and CAPES (Ciencia do Mar II).

REFERENCES CITED

Adatte, T., Keller, G., and Stinnesbeck, W., 2002, Late Cretaceous to early Paleocene climate and sea-level fluctuations: The Tunisian record: Palaeogeography, Palaeoclimatology, Palaeoecology, v. 178, p. 165–196, doi:10.1016/S0031-0182(01)00395-9.

Alvarez, L.W., and Lowrie, W., 1984, Magnetic stratigraphy applied to synsedimentary slumps, turbidites, and basin analysis: The Scaglia Limestone at Furlo (Italy): Geological Society of America Bulletin, v. 95, p. 324–336, doi:10.1130/0016-7606(1984)95<324:MSATSS>2.0.CO;2.

Alvarez, L.W., Alvarez, W., Asaro, F., and Michel, H.V., 1980, Extraterrestrial cause for the Cretaceous-Tertiary extinction: Science, v. 208, no. 4448, p. 1095–1108, doi:10.1126/science.208.4448.1095.

Alvarez, W., Colacicchi, R., and Montanari, A., 1985, Synsedimentary slides and bedding formation in Apennines pelagic limestones: Journal of Sedimentary Research, v. 55, p. 720–734, doi:10.1306/212F87CE-2B24-11D7-8648000102C1865D.

Arenillas, I., Arz, J.A., Grajales-Nishimura, J.M., Murillo-Muñetón, G., Alvarez, W., Camargo-Zaroguera, A., Molina, E., and Rosales-Dominguez, C., 2006, Chicxulub impact event is Cretaceous/Paleogene boundary in age: New micropaleontological evidence: Earth and Planetary Science Letters, v. 249, p. 241–257, doi:10.1016/j.epsl.2006.07.020.

Arthur, M.A., and Fischer, A., 1977, Upper Cretaceous–Paleocene magnetic stratigraphy at Gubbio, Italy. I. Lithostratigraphy and sedimentology: Geological Society of America Bulletin, v. 88, p. 367–371, doi:10.1130/0016-7606(1977)88<367:UCMSAG>2.0.CO;2.

Batenburg, S.J., Sprovieri, M., Gale, A.S., Hilgen, F.J., Hüsing, S., Laskar, J., Liebrand, D., Lirer, F., Orue-Etxebarria, X., Pelosi, N., and Smit, J., 2012, Cyclostratigraphy and astronomical tuning of the late Maastrichtian at Zumaia (Basque country, northern Spain): Earth and Planetary Science Letters, v. 359–360, p. 264–278, doi:10.1016/j.epsl.2012.09.054.

Batenburg, S.J., De Vleeschouwer, D., Sprovieri, M., Hilgen, F.J., Gale, A.S., Singer, B.S., Koeberl, C., Coccioni, R., Claeys, P., and Montanari, A., 2016, Orbital control on the timing of oceanic anoxia in the Late Cretaceous: Climate of the Past, doi:10.5194/cp-2015-182.

Beaudoin, B., M'Ban, E.P., Montanari, A., and Pinault, M., 1996, Stratigraphie haute resolution (<20 ka) dans le Cenomanien du bassin de Marches-Ombrie (Italie): Paris, Académie de Sciences Comptes Rendus, v. 323, p. 689–696.

Bice, D., Montanari, A., and Rusciadelli, G., 2007, Earthquake-induced turbidites triggered by seal level oscillations in the Upper Cretaceous and Paleocene of Italy: Terra Nova, v. 19, p. 387–392, doi:10.1111/j.1365-3121.2007.00752.x.

Bice, D., Montanari, A., Vucetić, V., and Vucetić, M., 2012, The influence of regional and global climatic oscillations on Croatian climate: International Journal of Climatology, v. 32, p. 1537–1557, doi:10.1002/joc.2372.

Brown, R., Koeberl, C., Montanari, A., and Bice, D., 2009, Cyclostratigraphic analysis and astronomical tuning of the Eocene-Oligocene boundary GSSP at Massignano (Italy), *in* Koeberl, C., and Montanari, M., eds., The Late Eocene Earth—Hothouse, Icehouse, and Impacts: Geological Society of America Special Paper 452, p. 119–137, doi:10.1130/2009.2452(08).

Bush, A.B.G., and Philander, S.G.H., 1997, The late Cretaceous: Simulation with a coupled atmosphere-ocean general circulation model: Paleoceanography, v. 12, p. 495–516, doi:10.1029/97PA00721.

Channell, J.E.T., D'Argenio, B., and Horvath, F., 1979, Adria, the African promontory in Mesozoic Mediterranean palaeogeography: Earth-Science Reviews, v. 15, p. 213–292, doi:10.1016/0012-8252(79)90083-7.

Chenet, A.-L., Quidelleur, X., Fluteau, F., Courtillot, V., and Bajpai, S., 2007, ^{40}K-^{40}Ar dating of the Main Deccan large igneous province: Further evidence of KTB age and short duration: Earth and Planetary Science Letters, v. 263, p. 1–15, doi:10.1016/j.epsl.2007.07.011.

Claussen, M., 1997, Modeling bio-geophysical feedback in the African and Indian monsoon region: Climate Dynamics, v. 13, p. 247–257, doi:10.1007/s003820050164.

Cleaveland, L.C., Jensen, J., Goese, S., Bice, D.M., and Montanari, A., 2002, Cyclostratigraphic analysis of pelagic carbonates at Monte dei Corvi (Ancona, Italy) and astronomical correlation of the Serravalian-Tortonian boundary: Geology, v. 30, p. 931–934, doi:10.1130/0091-7613(2002)030<0931:CAOPCA>2.0.CO;2.

Coccioni, R., and Premoli Silva, I., 2015, Revised upper Albian–Maastrichtian calcareous plankton biostratigraphy and magneto-stratigraphy of the

classical Tethyan Gubbio section (Italy): Newsletters on Stratigraphy, v. 48, p. 47–90, doi:10.1127/nos/2015/0055.

Coccioni, R., Frontalini, F., Bancalà, G., Fornaciari, E., Jovane, L., and Sprovieri, M., 2010, The Dan-C2 hyperthermal event at Gubbio (Italy): Global implications, environmental effects, and cause(s): Earth and Planetary Science Letters, v. 297, p. 298–305, doi:10.1016/j.epsl.2010.06.031.

Coccioni, R., Bancalà, G., Catanzarit, R., Fornaciari, E., Frontalini, F., Giusberti, L., Jovane, L., Luciani, V., Savian, J., and Sprovieri, M., 2012a, An integrated stratigraphic record of the Palaeocene–lower Eocene at Gubbio (Italy): New insights into the early Palaeogene hyperthermals and carbon isotope excursions: Terra Nova, v. 24, p. 380–386, doi:10.1111/j.1365-3121.2012.01076.x.

Coccioni, R., Sideri, M., Bancala, G., Catanzariti, R., Frontalini, F., Jovane, L., Montanari, A., and Savain, J., 2012b, Integrated stratigraphy (magneto-, bio- and chronostratigraphy) and geochronology of the Palaeogene pelagic succession of the Umbria-Marche Basin (central Italy), *in* Jovane, L., Herrero-Bervera, E., Hinnov, L.A., and Housen, B.A., eds., Magnetic Methods and the Timing of Geological Processes: Geological Society, London, Special Publication 373, p. 111–131, doi:10.1144/SP373.4.

Coccioni, R., Catanzariti, R., Frontalini, F., Galbrun, B., Jovane, L., Montanari, A., Savian, J., and Sideri, M., 2016, Integrated magnetostratigraphy, biostratigraphy, and chronostratigraphy of the Paleogene pelagic succession at Gubbio (central Italy), *in* Menichetti, M., Coccioni, R., and Montanari, A., eds., The Stratigraphic Record of Gubbio: Integrated Stratigraphy of the Late Cretaceous–Paleogene Umbria-Marche Pelagic Basin: Geological Society of America Special Paper 524, doi:10.1130/2016.2524(10).

Courtillot, V.E., and Renne, P.R., 2003, On the ages of flood basalt events: Comptes Rendus Geoscience, v. 335, p. 113–140, doi:10.1016/S1631-0713(03)00006-3.

Coxall, H.K., D'Hondt, S., and Zachos, J.C., 2006, Pelagic evolution and environmental recovery after the Cretaceous-Paleogene mass extinction: Geology, v. 34, p. 297–300, doi:10.1130/G21702.1.

Cramer, B.S., Wright, J.D., Kent, J.D., and Aubry, M.-P., 2003, Orbital climate forcing of $\delta^{13}C$ excursions in the late Paleocene–early Eocene (chrons C24n-C25n): Paleoceanography, v. 18, 1097, p. 21-1–21-25, doi:10.1029/2003PA000909.

Dercourt, J., Ricou, L.E., and Vrielynck, B., 1993, Atlas Tethys Palaeoenvironmental Maps: Paris, Gauthier Villars, 307 p.

D'Hondt, S., 2005, Consequences of the Cretaceous/Paleogene mass extinction for marine ecosystems: Annual Review of Ecology Evolution and Systematics, v. 36, p. 295–317, doi:10.1146/annurev.ecolsys.35.021103.105715.

D'Hondt, S., Donaghay, P., Zachos, J.C., Luttenberg, D., and Lindinger, M., 1998, Organic carbon fluxes and ecological recovery from the Cretaceous-Tertiary mass extinction: Science, v. 282, no. 5387, p. 276–279, doi:10.1126/science.282.5387.276.

Dinarès-Turell, J., Westerhold, T., Pujalte, V., Röhl, U., and Kroon, D., 2014, Astronomical calibration of the Danian stage (early Paleocene) revisited: Settling chronologies of sedimentary records across the Atlantic and Pacific Oceans: Earth and Planetary Science Letters, v. 405, p. 119–131, doi:10.1016/j.epsl.2014.08.027.

Galeotti, S., Moretti, M., Cappelli, C., Phillips, J., Lanci, L., Littler, K., Monechi, S., Petrizzo, M.R., Premoli Silva, I., and Zachos, J.C., 2015, The Bottaccione section at Gubbio, central Italy: A classical Paleocene Tethyan setting revisited: Newsletters on Stratigraphy, v. 48, p. 325–339, doi:10.1127/nos/2015/0067.

Ganopolski, A., Kubatzki, C., Claussen, M., Brovkin, V., and Petoukhov, V., 1998, The influence of vegetation-atmosphere-ocean interaction on climate during the mid-Holocene: Science, v. 280, no. 5371, p. 1916–1919, doi:10.1126/science.280.5371.1916.

Gardin, S., Galbrun, B., Thibault, N., Coccioni, R., and Premoli Silva, I., 2012, Bio-magnetostratigraphy for the upper Campanian–Maastrichtian from the Gubbio area, Italy: New results from the Contessa Highway and Bottaccione sections: Newsletters on Stratigraphy, v. 45, p. 75–103, doi:10.1127/0078-0421/2012/0014.

Gradstein, F., Ogg, J., and Smith, A., eds., 2004, A Geological Time Scale 2004: Cambridge, Cambridge University Press, 610 p.

Gradstein, F., Ogg, J., Schmitz, M., and Ogg., G., eds., 2012, The Geological Time Scale 2012: Oxford, Elsevier, 1176 p., doi:10.1016/B78-0-444-59425-9.00004-4

Hay, W.W., DeConto, R.M., Wold, C.N., Wilson, K.M., Voigt, S., Schulz, M., Wold, A.R., Dullo, W.-C., Ronov, A.B., Balukhovsky, A.N., and Södinget, E., 1999, Alternative global Cretaceous paleogeography, *in* Barrera, E., and Johnson, C., eds., Evolution of the Cretaceous Ocean-Climate System: Geological Society of America Special Paper 332, p. 1–47, doi:10.1130/0-8137-2332-9.1.

Herbert, T.D., and D'Hondt, S., 1990, Precessional climate cyclicity in Late Cretaceous–early Tertiary marine sediments: A high resolution chronometer of Cretaceous-Tertiary boundary events: Earth and Planetary Science Letters, v. 99, p. 263–275, doi:10.1016/0012-821X(90)90115-E.

Hildebrand, A.R., Penfield, G.T., Kring, D.A., Pilkington, M., Camargo, A., Jacobsen, S.B., and Boynton, W.V., 1991, Chicxulub crater: A possible Cretaceous/Tertiary boundary impact crater on the Yucatan Peninsula, Mexico: Geology, v. 19, p. 867–871, doi:10.1130/0091-7613(1991)019<0867:CCAPCT>2.3.CO;2.

Huber, B.T., MacLeod, K.G., and Norris, R.D., 2002, Abrupt extinction and subsequent reworking of Cretaceous planktonic foraminifera across the Cretaceous-Tertiary boundary: Evidence from the subtropical North Atlantic, *in* Koeberl, C., and MacLeod, K.G., eds., Catastrophic Events and Mass Extinctions: Impacts and Beyond: Geological Society of America Special Paper 356, p. 277–289, doi:10.1130/0-8137-2356-6.277.

Hunter, S.J., Haywood, A.M., Valdes, P.J., Francis, J.E., and Pound, M.J., 2013, Modelling equable climates of the Late Cretaceous: Can new boundary conditions resolve data-model discrepancies?: Palaeogeography, Palaeoclimatology, Palaeoecology, v. 392, p. 41–51, doi:10.1016/j.palaeo.2013.08.009.

Husson, D., Galbrun, B., Gardin, S., and Thibault, N., 2014, Tempo and duration of short-term environmental perturbations across the Cretaceous-Paleogene boundary: Stratigraphy, v. 11, p. 159–171.

Hyland, E., Murphy, B., Varela, P., Marks, K., Colwell, L., Tori, F., Monechi, S., Cleaveland, L., Brinkhuis, H., van Mourik, C., Coccioni, R., Bice, D., and Montanari, A., 2009, Integrated stratigraphic and astrochronologic calibration of the Eocene-Oligocene transition in the Monte Cagnero section (northeastern Apennines, Italy): A potential parastratotype for the Massignano global stratotype section and point (GSSP), *in* Koeberl, C., and Montanari, M., eds., The Late Eocene Earth—Hothouse, Icehouse, and Impacts: Geological Society of America Special Paper 452, p. 303–322, doi:10.1130/2009.2452(19).

Johnsson, M.J., and Reynolds, R.C., 1986, Clay mineralogy of shale-limestone rhythmites in the Scaglia Rossa (Turonian-Eocene), Italian Apennines: Journal of Sedimentary Petrology, v. 56, p. 501–509.

Keller, G., Adatte, T., Bhowmick, P.K., Upadhyay, H., Dave, A., Reddy, A.N., and Jaiprakash, B.C., 2012, Nature and timing of extinctions in Cretaceous-Tertiary planktic foraminifera preserved in Deccan intertrappean sediments of the Krishna-Godavari Basin, India: Earth and Planetary Science Letters, v. 341–344, p. 211–221, doi:10.1016/j.epsl.2012.06.021.

Kröpelin, S., Verschuren, D., Lézine, A.-M., Eggermont, H., Cocquyt, C., Francus, P., Cazet, J.-P., Fagot, M., Rumes, B., Russell, J.M., Darius, F., Conley, D.J., Schuster, M., von Suchodoletz, H., and Engstrom, D.R., 2008, Climate-driven ecosystem succession in the Sahara: The past 6000 years: Science, v. 320, no. 5877, p. 765–768, doi:10.1126/science.1154913.

Kutzbach, J.E., 1981, Monsoon climate of the early Holocene: Climate experiment with the Earth's orbital parameters for 9000 years ago: Science, v. 214, no. 4516, p. 59–61, doi:10.1126/science.214.4516.59.

Kutzbach, J.E., and Liu, Z., 1997, Response of the African monsoon to orbital forcing and ocean feedbacks in the middle Holocene: Science, v. 278, no. 5337, p. 440–443, doi:10.1126/science.278.5337.440.

Laskar, J., Robutel, P., Joutel, F., Gastineau, M., Correia, A.C.M., and Levrard, B., 2004, A long-term numerical solution for the insolation quantities of the Earth: Astronomy & Astrophysics, v. 428, p. 261–285, doi:10.1051/0004-6361:20041335.

Laskar, J., Fienga, A., Gastineau, M., and Manche, H., 2011, La2010: A new orbital solution for the long-term motion of the Earth: Astronomy & Astrophysics, v. 532, 15 p., doi:10.1051/0004-6361/201116836.

Lourens, L., Sluijs, A., Kroon, D., Zachos, J.C., Thomas, E., Röhl, U., Bowles, J., and Raffi, I., 2005, Astronomical pacing of late Palaeocene to early Eocene global warming events: Nature, v. 435, p. 1083–1087, doi:10.1038/nature03814.

Lowrie, W., Alvarez, W., Napoleone, G., Perch-Nielsen, K., Premoli Silva, I., and Toumarkine, M., 1982, Paleogene magnetic stratigraphy in Umbrian pelagic carbonate rocks: The Contessa sections, Gubbio: Geological Society of America Bulletin, v. 93, p. 414–432, doi:10.1130/0016-7606(1982)93<414:PMSIUP>2.0.CO;2.

Lowrie, W., Alvarez, W., and Asaro, F., 1990, The origin of the White Beds below the Cretaceous-Tertiary boundary in the Gubbio section, Italy: Earth and Planetary Science Letters, v. 98, p. 303–312, doi:10.1016/0012-821X(90)90032-S.

Luterbacher, H.P., and Premoli Silva, I., 1964, Biostratigrafia del limite creteceo-terziario nell'Appennino central: Rivista Italiana Paleontologia e Stratigrafia, v. 70, p. 67–128.

Mader, D., Cleaveland, L., Bice, D., Montanari, A., and Koeberl, C., 2004, High-resolution geochemical proxies of a short Langhian pelagic sequence at the Cònero Riviera, Ancona (Italy): Some palaeoenvironmental and cyclostratigraphic considerations: Palaeogeography, Palaeoclimatology, Palaeoecology, v. 211, p. 325–344, doi:10.1016/j.palaeo.2004.06.001.

Miller, K.G., Wright, J.D., and Browning, J.V., 2005, Visions of ice sheets in a greenhouse world: Marine Geology, v. 217, p. 215–231, doi:10.1016/j.margeo.2005.02.007.

Mitchell, R.N., Bice, D.M., Montanari, A., Cleaveland, L.C., Christianson, K.T., Coccioni, R., and Hinnov, L.A., 2008, Oceanic anoxic events? Orbital prelude to the Bonarelli Level (OAE 2): Earth and Planetary Science Letters, v. 267, p. 1–16, doi:10.1016/j.epsl.2007.11.026.

Montanari, A., Chan, L.S., and Alvarez, W., 1989, Synsedimentary tectonics in the Late Cretaceous–early Tertiary pelagic basin of the Northern Apennines, *in* Crevello, P., Wilson, J.L., Sarg, R., and Reed, F., eds., Controls on Carbonate Platforms and Basin Development: Society of Economic Paleontologists and Mineralogists Special Publication 44, p. 379–399, doi:10.2110/pec.89.44.0379.

Mukhopadhyay, S., Farley, K.A., and Montanari, A., 2001, A short duration of the Cretaceous-Tertiary boundary event: Evidence from extraterrestrial helium-3: Science, v. 291, no. 5510, p. 1952–1955, doi:10.1126/science.291.5510.1952.

Muller, R.A., and MacDonald, G.J., 2000, Ice Ages and Astronomical Causes: Data, Spectral Analysis and Mechanisms: London, Springer, 318 p.

Nordt, L., Atchley, S., and Dworkin, S., 2003, Terrestrial evidence for two greenhouse events in the latest Cretaceous: GSA Today, v. 13, no. 12, p. 4–9, doi:10.1130/1052-5173(2003)013<4:TEFTGE>2.0.CO;2.

Odin, G.S., Hurford, A.J., and Montanari, A., 1992, Study of a presumably volcano-sedimentary layer near the Cretaceous-Paleogene boundary in the Central Apennines (Italy), *in* Odin, G.S., ed., Phanerozoic Time Scale: International Union of Geological Sciences Subcommission on Geochronology Bulletin de Liaison, v. 11, p. 26–28.

Olsson, R.K., Liu, C., and Van Fossen, M., 1996, The Cretaceous-Tertiary catastrophic event at Millers Ferry, Alabama, *in* Ryder, G., Fastovsky, D.E., and Gartner, S., eds., The Cretaceous-Tertiary Event and Other Catastrophes in Earth History: Geological Society of America Special Paper 307, p. 263–277, doi:10.1130/0-8137-2307-8.263.

Pälike, H., Norris, R.D., Herrle, J.O., Wilson, P.A., Coxall, H.A., Lear, C.H., Shackleton, N.J., Tripati, A.K., and Wade, B.S., 2006, The heartbeat of the Oligocene: Science, v. 314, no. 5807, p. 1894–1898, doi:10.1126/science.1133822.

Park, J., and Oglesby, R.J., 1991, Milankovitch rhythms in the Cretaceous: A GCM modeling study: Palaeogeography, Palaeoclimatology, Palaeoecology, v. 90, p. 329–355, doi:10.1016/S0031-0182(12)80034-4.

Pey, J., Querol, X., Alastuey, A., Forastiere, F., and Stafoggia, M., 2013, African dust outbreaks over the Mediterranean Basin during 2001–2011: PM10 concentrations, phenomenology and trends, and its relation with synoptic and mesoscale meteorology: Atmospheric Chemistry and Physics, v. 13, p. 1395–1410, doi:10.5194/acp-13-1395-2013.

Price, G.D., and Nunn, E.V., 2010, Valangian isotope variation in glendonites and belemnites from Arctic Svalbard: Transient glacial temperatures during the Cretaceous greenhouse: Geology, v. 38, p. 251–254, doi:10.1130/G30593.1.

Prospero, J.M., Glaccum, R.A., and Nees, R.T., 1981, Atmospheric transport of soil dust from Africa to South America: Nature, v. 289, p. 570–572, doi:10.1038/289570a0.

Ravizza, G., 2007, Reconstructing the marine $^{187}Os/^{188}Os$ record and the particulate flux of meteoritic osmium during the Late Cretaceous: Geochimica et Cosmochimica Acta, v. 71, p. 1355–1369, doi:10.1016/j.gca.2006.11.006.

Ravizza, G., and Peucker-Ehrenbrink, B., 2003, Chemostratigraphic evidence of Deccan volcanism from the marine isotope record: Science, v. 302, no. 5649, p. 1392–1395, doi:10.1126/science.1089209.

Renne, P.R., Deino, A.L., Hilgen, F.J., Kuiper, K.F., Mark, D.F., Mitchell, W.S., III, Morgan, L.E., Mundil, R., and Smit, J., 2013, Time scales of critical events around the Cretaceous-Paleogene boundary: Science, v. 339, no. 6120, p. 684–687, doi:10.1126/science.1230492.

Robinson, N., Ravizza, G., Coccioni, R., Peucker-Ehrenbrink, B., and Norris, R., 2009, A high-resolution marine $^{187}Os/^{188}Os$ record for the late Maastrichtian: Distinguishing the chemical fingerprints of Deccan volcanism and the KP impact event: Earth and Planetary Science Letters, v. 281, p. 159–168, doi:10.1016/j.epsl.2009.02.019.

Roggenthen, W.M., and Napoleone, G., 1977, Upper Cretaceous–Paleocene magnetic stratigraphy at Gubbio, Italy. IV. Upper Maastrichtian–Paleocene magnetic stratigraphy: Geological Society of America Bulletin, v. 88, p. 378–382, doi:10.1130/0016-7606(1977)88<378:UCMSAG>2.0.CO;2.

Rosenbaum, G., Lister, G.S., and Dubois, C., 2002, Reconstruction of the tectonic evolution of the western Mediterranean since the Oligocene: Journal of the Virtual Explorer, v. 8, p 107–130, doi:10.3809/jvirtex.2002.00053.

Russon, T., Paillard, D., and Elliot, E., 2010, Potential origins of 400–500 kyr periodicities in the ocean carbon cycle: A box model approach: Global Biogeochemical Cycles, v. 24, GB2013, doi:10.1029/2009GB003586.

Schoene, B., Samperton, K.M., Eddy, M.P., Keller, G., Adatte, T., Bowring, S.A., Khadri, S.F.R., and Gertch, B., 2015, U-Pb geochronology of the Deccan Traps and relation to the end-Cretaceous mass extinction: Science, v. 347, no. 6218, p. 182–184, doi:10.1126/science.aaa0118.

Schulte, P., et al., 2010, The Chicxulub asteroid impact and mass extinction at the Cretaceous-Paleogene boundary: Science, v. 327, no. 5970, p. 1214–1218, doi:10.1126/science.1177265.

Self, S., Blake, S., Sharma, K., Widdowson, M., and Sephton, S., 2008, Sulfur and chlorine in Late Cretaceous Deccan magmas and eruptive gas release: Science, v. 319, no. 5870, p. 1654–1657, doi:10.1126/science.1152830.

Smit, J., 1982, Extinction and evolution of planktonic foraminifera after a major impact at the Cretaceous/Tertiary boundary, *in* Silver, L.T., and Schultz, P.H., eds., Geological Implications of Impacts of Large Asteroids and Comets on the Earth: Geological Society of America Special Paper 190, p. 329–352, doi:10.1130/SPE190-p329.

Smit, J., and Hertogen, J., 1980, An extraterrestrial event at the Cretaceous-Tertiary boundary: Nature, v. 285, p. 198–200, doi:10.1038/285198a0.

Swisher, C.C., Grajales-Nishimura, J.M., Montanari, A., Margolis, S.V., Claeys, P., Alvarez, W., Renne, P., Cedillo-Pardo, E., Maurrasse, F., Curtis, G., Smit, J., and McWilliams, M.O., 1992, Coeval $^{40}Ar/^{39}Ar$ ages of 65.0 million years ago from Chicxulub crater melt rock and Cretaceous-Tertiary boundary tektites: Science, v. 257, no. 5072, p. 954–958, doi:10.1126/science.257.5072.954.

Tuenter, E., Weber, S.L., Hilgen, F.J., and Lourens, L.J., 2003, The response of the African summer monsoon to remote and local forcing due to precession and obliquity: Global and Planetary Change, v. 36, p. 219–235, doi:10.1016/S0921-8181(02)00196-0.

Tuenter, E., Weber, S.L., Hilgen, F.J., Lourens, L.J., and Ganopolski, A., 2005, Simulation of climate phase lags in response to precession and obliquity forcing and the role of vegetation: Climate Dynamics, v. 24, p. 279–295, doi:10.1007/s00382-004-0490-1.

Upchurch, G.R., Otto-Bliesner, B.L., and Scotese, C.R., 1999, Terrestrial vegetation and its effects on climate during the latest Cretaceous, *in* Barrera, E., and Johnson, C., eds., Evolution of the Cretaceous Ocean-Climate System: Geological Society of America Special Paper 332, p. 407–426, doi:10.1130/0-8137-2332-9.407.

Voigt, S., Gale, A.S., Jung, C., and Jenkyns, H.C., 2012, Global correlation of upper Campanian–Maastrichtian successions using carbon-isotope stratigraphy: Development of a new Maastrichtian timescale: Newsletters on Stratigraphy, v. 45, p. 25–53, doi:10.1127/0078-0421/2012/0016.

Wendler, I., 2013, A critical evaluation of carbon isotope stratigraphy and biostratigraphic implications for Late Cretaceous global correlation: Earth-Science Reviews, v. 126, p. 116–146, doi:10.1016/j.earscirev.2013.08.003.

Wilf, P., Johnson, K.R., and Huber, B.T., 2003, Correlated terrestrial and marine evidence for global climate changes before mass extinction at the Cretaceous-Paleogene boundary: National Academy of Sciences Proceedings, v. 100, p. 599–604, doi:10.1073/pnas.0234701100.

Zachos, C.J., McCarren, H., Murphy, B., Röhl, U., and Westerhold, T., 2010, Tempo and scale of the late Paleocene and early Eocene carbon isotope cycles: Implications for the origin of hyperthermals: Earth and Planetary Science Letters, v. 299, p. 242–249, doi:10.1016/j.epsl.2010.09.004.

Manuscript Accepted by the Society 15 March 2016

Printed in the USA